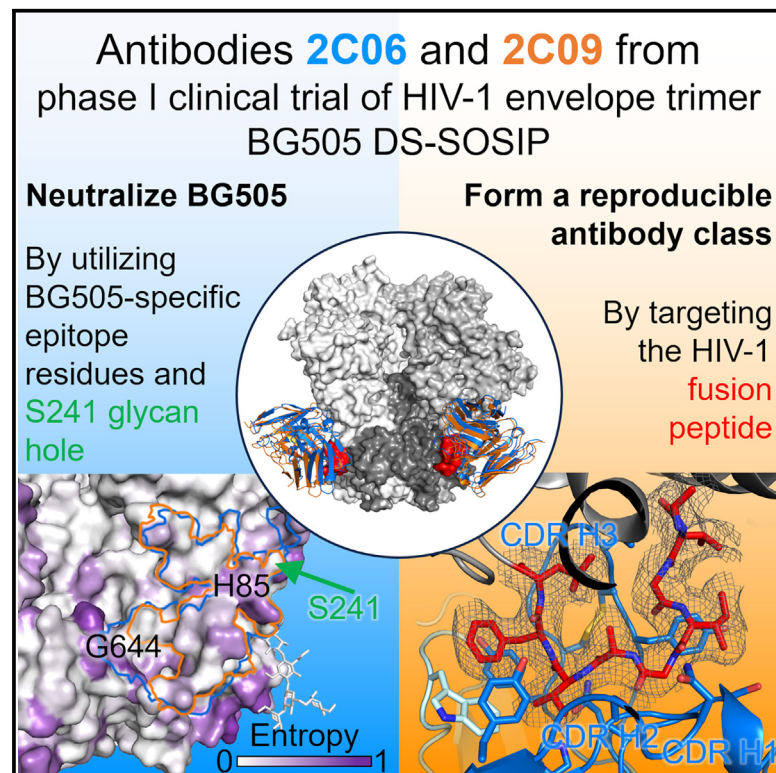


# HIV-1 neutralizing antibodies elicited in humans by a prefusion-stabilized envelope trimer form a reproducible class targeting fusion peptide

## Graphical abstract



## Authors

Shuishu Wang, Flavio Matassoli, Baoshan Zhang, ..., Daniel C. Douek, Adrian B. McDermott, Peter D. Kwong

## Correspondence

pdkwong@nih.gov

## In brief

Vaccine elicitation of tier-2 HIV-1 neutralizing antibodies in humans has been a long-sought goal. Wang et al. isolate and determine structures of two antibodies from a clinical trial of a prefusion-closed HIV-1 envelope trimer. These antibodies target the fusion-peptide site of vulnerability, form a reproducible class, and neutralize the tier-2 HIV-1 strain BG505.

## Highlights

- HIV-1 neutralizing antibodies 2C06 and 2C09 from VRC 018 clinical trial are isolated
- Cryo-EM structures of 2C06 and 2C09 in complex with HIV envelope trimer are determined
- 2C06 and 2C09 binding requires a glycan hole at 241 and BG505-specific residues
- Antibodies 2C06 and 2C09 form a reproducible class, recognizing fusion peptide



## Article

# HIV-1 neutralizing antibodies elicited in humans by a prefusion-stabilized envelope trimer form a reproducible class targeting fusion peptide

Shuishu Wang,<sup>1</sup> Flavio Matassoli,<sup>1</sup> Baoshan Zhang,<sup>1</sup> Tracy Liu,<sup>1</sup> Chen-Hsiang Shen,<sup>1</sup> Tatsiana Bylund,<sup>1</sup> Timothy Johnston,<sup>1</sup> Amy R. Henry,<sup>1</sup> I-Ting Teng,<sup>1</sup> Prabhanshu Tripathi,<sup>1</sup> Jordan E. Becker,<sup>2,3</sup> Anita Changela,<sup>1</sup> Ridhi Chaudhary,<sup>1</sup> Cheng Cheng,<sup>1</sup> Martin Gaudinski,<sup>1</sup> Jason Gorman,<sup>1</sup> Darcy R. Harris,<sup>1</sup> Myungjin Lee,<sup>1</sup> Nicholas C. Morano,<sup>2,3</sup> Laura Novik,<sup>1</sup> Sijy O'Dell,<sup>1</sup> Adam S. Olia,<sup>1</sup> Danealle K. Parchment,<sup>1</sup> Reda Rawi,<sup>1</sup> Jesmine Roberts-Torres,<sup>1</sup> Tyler Stephens,<sup>4</sup> Yaroslav Tsybovsky,<sup>4</sup> Danyi Wang,<sup>1</sup> David J. Van Wazer,<sup>1</sup> Tongqing Zhou,<sup>1</sup> Nicole A. Doria-Rose,<sup>1</sup> Richard A. Koup,<sup>1</sup> Lawrence Shapiro,<sup>2,3</sup> Daniel C. Douek,<sup>1</sup> Adrian B. McDermott,<sup>1</sup> and Peter D. Kwong<sup>1,3,5,\*</sup>

<sup>1</sup>Vaccine Research Center, National Institutes of Health, Bethesda, MD 20892, USA

<sup>2</sup>Zuckerman Mind Brain Behavior Institute, Columbia University, New York, NY 10027, USA

<sup>3</sup>Department of Biochemistry and Molecular Biophysics, Columbia University Vagelos College of Physicians and Surgeons, New York, NY 10032, USA

<sup>4</sup>Electron Microscopy Laboratory, Cancer Research Technology Program, Frederick National Laboratory for Cancer Research, Frederick, MD 21701, USA

<sup>5</sup>Lead contact

\*Correspondence: [pdkwong@nih.gov](mailto:pdkwong@nih.gov)

<https://doi.org/10.1016/j.celrep.2023.112755>

## SUMMARY

Elicitation of antibodies that neutralize the tier-2 neutralization-resistant isolates that typify HIV-1 transmission has been a long-sought goal. Success with prefusion-stabilized envelope trimers eliciting autologous neutralizing antibodies has been reported in multiple vaccine-test species, though not in humans. To investigate elicitation of HIV-1 neutralizing antibodies in humans, here, we analyze B cells from a phase I clinical trial of the “DS-SOSIP”-stabilized envelope trimer from strain BG505, identifying two antibodies, N751-2C06.01 and N751-2C09.01 (named for donor-lineage.clone), that neutralize the autologous tier-2 strain, BG505. Though derived from distinct lineages, these antibodies form a reproducible antibody class that targets the HIV-1 fusion peptide. Both antibodies are highly strain specific, which we attribute to their partial recognition of a BG505-specific glycan hole and to their binding requirements for a few BG505-specific residues. Prefusion-stabilized envelope trimers can thus elicit autologous tier-2 neutralizing antibodies in humans, with initially identified neutralizing antibodies recognizing the fusion-peptide site of vulnerability.

## INTRODUCTION

The HIV-1 envelope (Env) trimer is protected by multiple mechanisms of humoral evasion, including conformational masking, glycan shielding, and sequence variation.<sup>1–3</sup> While HIV-1 infection generally elicits autologous neutralizing antibodies<sup>4,5</sup>—and in a small fraction of individuals even broadly neutralizing antibodies<sup>6–12</sup>—Env-based immunization has generally yielded antibodies that are incapable of neutralizing the tier-2 neutralization-resistant strains of HIV-1 that typify natural transmission. A major roadblock has been trimer instability, with the prefusion mature Env trimer changing conformations and ultimately disassembling into constituent gp120 and gp41 subunits and in the process exposing immunodominant surfaces, which elicit poorly or non-neutralizing antibodies.

Stabilization of the Env trimer through the incorporation of a disulfide (SOS) between residues 501 of gp120 and 605 of

gp41 and the substitution of an isoleucine to a proline (IP) helped fix the trimer into a prefusion-closed conformation recognized by broadly neutralizing antibodies but not by non-neutralizing antibodies.<sup>13</sup> SOSIP-stabilized Env trimers could elicit autologous neutralizing antibodies in rabbits against diverse HIV strains,<sup>14</sup> including the clade A strain BG505 and the clade B strains B41 and AMC008. These often target glycan holes, such as at residues 241 and 289 in strain BG505.<sup>15,16</sup>

While vaccine elicitation of tier-2 neutralizing responses has now been reported in multiple vaccine-test species including non-human primates,<sup>17–19</sup> the characteristics of neutralizing antibodies elicited in humans by Env stabilized in a prefusion-closed conformation have not been reported. How does the human immune system respond to conformationally stabilized and highly glycosylated immunogens? Here, we analyze B cells from a phase I clinical trial (VRC 018) assessing a prefusion-stabilized Env trimer from strain BG505, fixed with an additional



disulfide (201C–433C) to comprise DS-SOSIP, which stays in a prefusion-closed conformation even in the presence of human CD4.<sup>20,21</sup> We sorted B cells with stabilized trimers with their bases covered with glycans and sequenced and expressed constituent antibodies, for which we assessed binding and neutralization. For antibodies capable of neutralizing the autologous strain, BG505, we determined cryo-electron microscopy (cryo-EM) structures with Env trimer. Collectively, the results reveal only a minority of responding B cells to be directed to the glycan-dense surface of the Env trimer versus its glycan-free base, and of these B cells, only ~1 in 100 bound with sufficient affinity to neutralize autologous virus; overall, we report Env-trimer vaccine-elicited antibodies from humans capable of neutralizing a tier-2 neutralization-resistant isolate to be strain-specific members of a reproducible class of antibodies, targeting the fusion-peptide site of vulnerability.

## RESULTS

### Sorting of VRC 018 B cells from donor N751 reveal that only a small fraction of elicited antibodies recognize the glycan-dense surface of the Env trimer

In the Vaccine Research Center (VRC) 018 clinical trial ([ClinicalTrials.gov](https://clinicaltrials.gov/ct2/show/study/NCT03783130) NCT03783130),<sup>22</sup> although no neutralization activity against the autologous BG505 strain was detected in serum samples, BG505 DS-SOSIP-specific antibody responses were elicited in all groups vaccinated with three 500- $\mu$ g doses of BG505 DS-SOSIP adjuvanted with alum at 2 weeks after regimen completion. This suggested that neutralizing antibodies might have been elicited, but at titers too low to be detected in bulk sera. To characterize vaccine-elicited antibodies, we sorted B cells from donor N751, which showed the highest BG505 DS-SOSIP-reactive ELISA responses in the 500- $\mu$ g intramuscular group of five participants<sup>22</sup> (Figures 1A, 1B, and S1). For sorting, we used a modified BG505 Env trimer with additional stabilization mutations<sup>23</sup> along with two engineered *N*-linked glycans per protomer, which were designed to cover the trimer base (hereafter referred to as glycan-base BG505 trimer, Figures S1A and S1B) to reduce the background of dominant base-targeting antibodies, allowing for the selection of antibodies binding to neutralizing epitopes on the Env trimer.

To quantify the number of cells binding to the glycan-dense Env-trimer surface relative to those bound the glycan-free base, we performed cell cytometry on immunoglobulin G-positive (IgG<sup>+</sup>) memory B cells (singlet, live, CD19<sup>+</sup>, CD3<sup>-</sup>, CD14<sup>-</sup>, CD56<sup>-</sup>, IgG<sup>+</sup>) from donor N751 (Figures S1C and S1D). Of antigen-positive memory B cells, 12.9% bound the glycan-base-covered BG505 versus 87.1% which bound only to BG505 with protein base. These data suggest that about 1 in 10 antigen-positive B cells could recognize the glycan-dense surface of the Env trimer.

From two plates of single-sorted B cells, 96 wells each, specific for the glycan-base BG505 trimer, we sequenced immunoglobulin genes and cloned them into an expression vector utilizing a method for rapid assembly, transfection, and production of immunoglobulins (RATP-Ig).<sup>25</sup> RATP-Ig supernatants were screened for binding to BG505 DS-SOSIP and glycan-base BG505 Env trimers by AlphaLISA, and we identified nine

double-positive B cell supernatants (Figure 1C). One of clones did not express in transient transfection of mammalian cells; the other eight were purified and confirmed by surface plasmon resonance (SPR) to bind glycan-base BG505 (dissociation constant [ $K_D$ ] values ranging from 2.86 to 17.6 nM) and BG505 DS-SOSIP ( $K_D$  values ranging from 0.46 to 2.28 nM) (Figure 1D). Overall, only a small fraction of the antigen-positive memory B cells encoded antibodies with moderate binding affinity to the non-base glycan-dense surface of the Env-trimer immunogen.

### Vaccine-elicited human antibodies N751-2C06.01 and N751-2C09.01 neutralize HIV strain BG505

We further characterized the purified antibodies for neutralization activity and found that the antibodies N751-2C06.01 and N751-2C09.01 (named for donor-lineage.clone, hereafter referred to as 2C06 and 2C09) neutralized both BG505 and a version of BG505 virus with glycan at residue 611 missing (BG505.N611Q), found to be especially sensitive to fusion-peptide-directed antibodies (Figures 1E, S2A, and S2B). Because of their ability to neutralize the BG505.N611Q virus, we tested antibodies 2C06 and 2C09 for their binding to the exposed N-terminal segment of the fusion peptide (Figure S2C). Both antibodies bound fusion peptide, and 2C06 had substantially reduced affinity to shorter peptides; 2C09 also showed reduced binding to shorter peptides, though not as significantly as 2C06. Both 2C06 and 2C09 competed with fusion-peptide-directed antibodies VRC34.01, PGT151, and vFP16.02 for binding to BG505 Env trimer (Figure S2D).

We used SPR to measure the binding of the antigen-binding fragments (Fabs) of 2C06 and 2C09 to BG505 DS-SOSIP trimer. Both bound tightly, with  $K_D$  of 3.91 and 5.40 nM for 2C06 and 2C09, respectively (Figure 1F). Overall, we identified two antibodies from the BG505 DS-SOSIP/alum clinical trial that neutralized wild-type BG505, appeared to be fusion-peptide directed, and bound BG505 Env trimer with nanomolar affinity.

### Cryo-EM structure of N751-2C06.01 in complex with BG505 DS-SOSIP reveals the antibody to bind at the fusion-peptide site of vulnerability

To define recognition details, we determined the cryo-EM structure of 2C06 in complex with BG505 DS-SOSIP. We obtained a 3D-reconstruction map at 2.95 Å from 645,442 particles utilizing C1 symmetry (Figure S3 and Table S1). Binding of 2C06 induced asymmetry in the trimer (Figure S3F); specifically, interactions of complementarity-determining region 3 of heavy chain (CDR H3) from two of the Fabs with the C-terminal helix of a neighboring gp41 subunit served to position this helix closer to the two Fabs and to the primary protomer. This movement of gp41 C-terminal helix was observed with two of the Fabs, not the third, and enabled the two N-terminal residues from the third fusion peptide (residues 512 and 513) to interact with the C-terminal helix of a neighboring gp41.

Antibody 2C06 bound at the fusion-peptide site of vulnerability (Figure 2A), with epitope analysis utilizing prior antibody-Env structural complexes<sup>26</sup> indicating substantial epitope overlap with VRC34.01 (71%) and lower epitope overlap with ACS202 (62%) and PGT151 (54%) (Table S2). Fusion-peptide residues 514–520 interacted almost exclusively with the heavy chain of

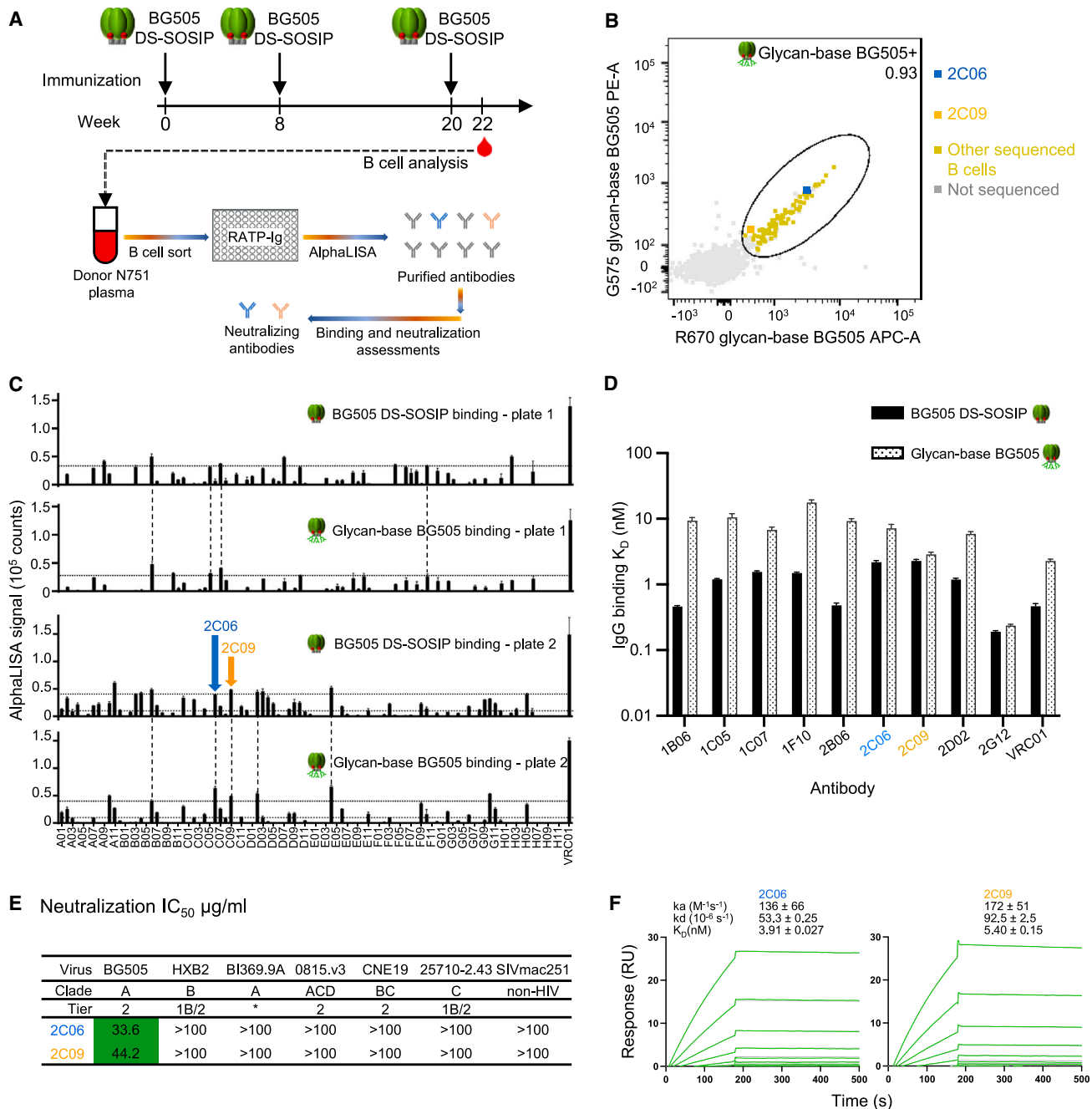


**Figure 1. Sorting of VRC 018 B cells from donor N751 identifies antibodies 2C06 and 2C09 that neutralize BG505**

(A) VRC 018 clinical regimen and a flowchart for B cell sorting and antibody screening.

(B) Single B cell sorting with glycan-base BG505 trimer probes reveals only a small fraction of memory B cells from VRC 018 clinical trial to be directed to the glycan-dense surface of the Env trimer versus its glycan-free base.

(C) AlphaLISA screening of RATP-Ig supernatants from sorted B cells for antibodies that bind both BG505 DS-SOSIP and glycan-base BG505. Data were measured in triplicates; error bars represent standard error of the mean (SEM).

(D) Apparent affinity measurement of top antibodies from AlphaLISA screening for binding to BG505 DS-SOSIP and glycan-base BG505 trimers. Antibody IgGs were expressed and purified, and their binding to trimers was measured by Cartera. 2G12 and VRC01 were used as positive controls. Motavizumab was used as negative control, and no binding was observed.

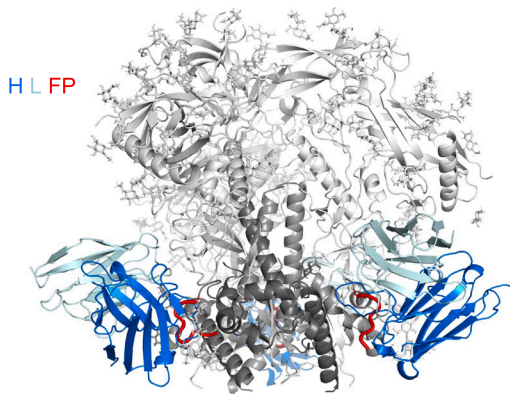
(E) Antibodies 2C06 and 2C09 neutralize BG505, but no other tested strains. Asterisk denotes tier status for BI369.9A unknown but resistant to antibodies 17b, 48d, F105, 3074, and 447-52D that neutralize only laboratory-adapted strains.<sup>24</sup> Neutralization for other antibodies from (D) that bind glycan-base BG505 are shown in Figure S2.

(F) Affinity of antibody Fabs binding to BG505 DS-SOSIP trimer, measured by SPR.

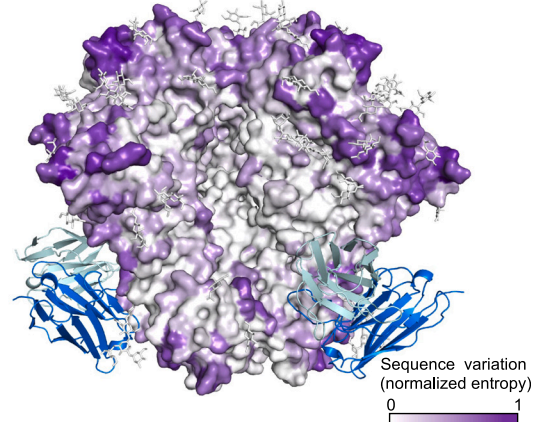
Data in (D) and (F) were measured once and the curves fitted with a simple 1:1 Langmuir binding model for the reported mean  $\pm$  SEM. See also Figures S1 and S2.



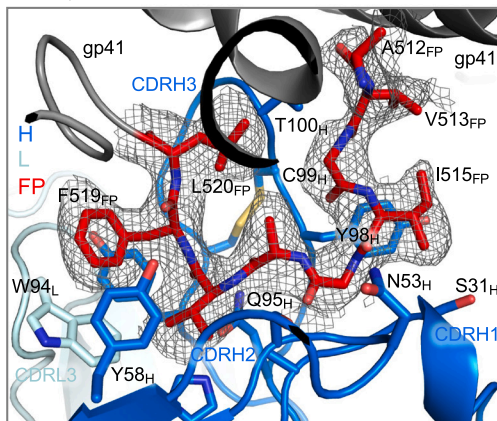
**A** Overall structure of 2C06



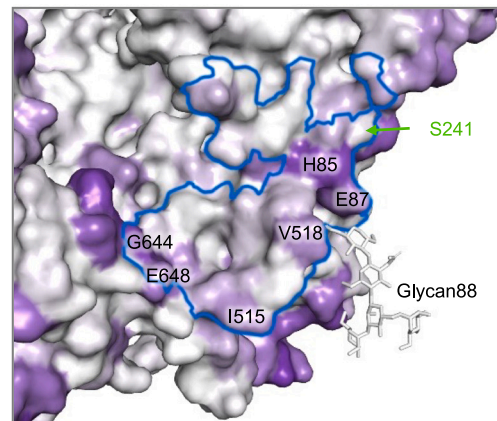
**D** HIV-1 group M Env sequence variation



**B** Density map at FP N-terminal residues



**E** Sequence conservation around 2C06 epitope



**C** Epitope with CDRs

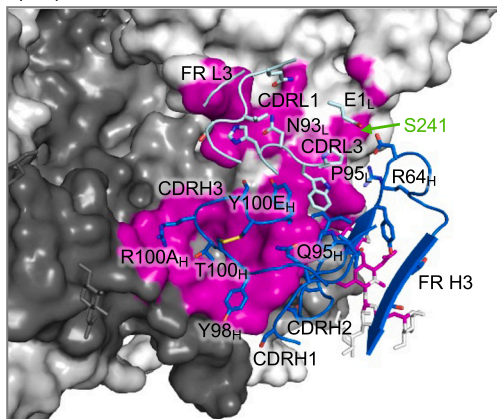


**Figure 2. Cryo-EM structure of N751-2C06.01 in complex with BG505 DS-SOSIP reveals antibody recognition at the fusion-peptide site of vulnerability**

(A) Cartoon representation of 2C06 in complex with BG505 DS-SOSIP. 2C06 bound at the fusion-peptide site and interacted with fusion peptide (FP), shown in red. Antibody heavy chain (H) is shown in blue, light chain (L) in pale cyan, gp41 in dark gray, and gp120 in light gray.

(B) Density map for fusion peptide N-terminal residues. The structure is shown in cartoon representation, with fusion peptide and antibody side chains interacting with fusion peptide shown in sticks. Color codes are as in (A).

(C) 2C06 epitope details. Env trimer is shown as surface with subunits in different shades of gray and the epitope surface in magenta. Antibody CDRs and FRs involved in binding are shown in cartoon representation, with interacting side chains shown in sticks. The glycan hole at S241 is on the edge of the epitope and is labeled.

(legend continued on next page)

2C06 (Figure 2B); these residues formed a U shape, looping back to interact with trimer. As mentioned above, at the binding sites where the 2C06 CDR H3 had less interaction with the neighboring gp41, the N-terminal two residues of the fusion peptide interacted with the C-terminal gp41 helix and were resolved with relatively weak electron density, whereas in the other two gp41 subunits the first two N-terminal residues of the fusion peptide did not have discernible electron density.

The fusion peptide was flanked by CDRs H1 and H2 on one side and CDR H3 on the other (Figure 2B), and its binding involved an average of  $\sim 470 \text{ \AA}^2$  of buried surface area (BSA) (Tables S3 and S4). CDR L3 had minor interactions with fusion-peptide residues 518 and 519 at  $\sim 60 \text{ \AA}^2$  BSA, and interactions with CDRs of heavy and light chains together accounted for nearly half of the total protein BSA of  $\sim 1,200 \text{ \AA}^2$ , of which more than  $800 \text{ \AA}^2$  were from the heavy chain. Light-chain interactions involved CDRs L1 and L3, framework region 3 (FR L3), and the side chain of its N-terminal residue (Figure 2C). Most light-chain interactions were with residues leading up to glycan at N88 (glycan88), which shared interactions with heavy chain, with glycan88 covering  $\sim 250 \text{ \AA}^2$  of heavy-chain BSA (Tables S3 and S4).

The 2C06 epitope also included S241, which is an *N*-glycosylation site in 97% of HIV isolates (<http://www.hiv.lanl.gov/content/index>), with BG505 being one of the rare strains with a glycan hole at 241 (Figure 2C and Table S5). HIV-1 group M Env surface residues are highly variable, especially at the apex (Figure 2D). However, the 2C06 epitope residues were mostly conserved, with only a few residues having significant entropy, such as H85, E87, G644, and E648 (Figure 2E). Most residues of the fusion peptide were well conserved except for I515 and V518, which have moderate entropy.

Overall, the cryo-EM structure of 2C06 in complex with BG505 DS-SOSIP revealed 2C06 to bind at the fusion-peptide site of vulnerability, with heavy-chain CDRs accounting for most of the interactions with the fusion peptide.

### Cryo-EM structure of N751-2C09.01 in complex with BG505 DS-SOSIP reveals epitope similarity to N751-2C06.01

To understand the differences and similarities between antibodies 2C06 and 2C09, we determined the cryo-EM structure of 2C09 in complex with BG505 DS-SOSIP. 2C09 binding to the envelope trimer did not induce noticeable asymmetry, and we obtained a 3D-reconstruction map at  $2.81 \text{ \AA}$  with C3 symmetry from 445,733 particles (Figure S4 and Table S1). Like 2C06, 2C09 bound at the fusion-peptide site of vulnerability (Figure 3A), with 90% overlap of the two epitopes.

The fusion peptide in the 2C09 bound complex also formed a U-shape conformation, except for its two N-terminal residues (512 and 513), which turned back to interact with antibody. As a result, fusion-peptide binding to 2C09 involved residues 512–

520 interacting almost exclusively with heavy-chain CDRs (Figure 3B), with  $\sim 470 \text{ \AA}^2$  of BSA (Tables S3 and S4). 2C09 interacted more extensively than 2C06 with the N-terminal residues of fusion peptide, providing an explanation for the stronger observed binding to shorter peptides by 2C09 versus 2C06 (Figure S2C). The 2C09 CDR L3 interacted with fusion-peptide residues 518 and 519, with  $\sim 90 \text{ \AA}^2$  BSA, from two tryptophan side chains, W94 and W96. The BSA with fusion peptide from CDRs of heavy and light chains together accounted for more than half of the total protein BSA of  $\sim 990 \text{ \AA}^2$  (not including BSA from the saccharide moiety at residue 88), a little less than that of 2C06.

The heavy chain of 2C09 contributed about 70% of the total epitope surface. The CDR H3 of 2C09 was four residues shorter than that of 2C06 and, unlike in the 2C06-Env complex, did not reach the neighboring gp41; this difference accounted for most of the difference in total BSA (Figures 3C and 3D). As such, the 2C09 epitope did not include residues G644 and E648, two of the high-entropy residues recognized by 2C06 on the neighboring protomer, but did include residues H85 and E87 (Figure 3D). Similar to 2C06, light-chain CDRs L1 and L3, and FR L3, were involved in trimer binding (Figure 3C), and most of the light-chain interactions were with residues 79–88. Binding to these residues was shared with the heavy chain and altogether accounted for  $\sim 280 \text{ \AA}^2$  BSA; interaction with glycan88 contributed an additional  $\sim 215 \text{ \AA}^2$  of heavy-chain BSA (Tables S3 and S4). The 2C09 epitope also recognized the S241 glycan hole (Figures 3C and 3D), in a manner similar to that of 2C06. Overall, the structure of 2C09 in complex with BG505 DS-SOSIP revealed a binding mode akin to that of 2C06 but with slightly reduced BSA due to a shorter CDR H3 (Figure 3E).

### Antibodies 2C06 and 2C09 form a reproducible antibody class

Antibodies 2C06 and 2C09 originated from similar heavy-chain variable genes, IGHV3-64D and IGHV3-64, respectively (Figures 4A and 4B). However, their heavy-chain D and J genes were different, indicating these two antibodies to be from two distinct lineages and resulting in different CDR H3 lengths. Among the 138 sequenced antibodies isolated from donor N751 using Env-trimer probes, IGHV3-64D accounted for  $\sim 4\%$ , whereas IGHV3-64 accounted for  $<1\%$  (Figure 4C and Table S6), indicating this similarity in V-gene usage to be unlikely to occur randomly; indeed, none of the other isolated antibodies that also bound both BG505 DS-SOSIP and glycan-base BG505 Env trimers derived from these heavy-chain V genes (Figures 1C and 1D; Table S6).

The similarity in origin genes and in Env-trimer recognition suggested that 2C06 and 2C09 might be members of a reproducible antibody class. Indeed, most residues involved in trimer binding were identical between 2C06 and 2C09, discounting the different length in CDR H3. Both 2C06 and 2C09 also showed

(D) Overall sequence variation of HIV-1 group M Env glycoproteins. Normalized sequence entropy is mapped on the trimer surface, with absolutely conserved residues (entropy of 0) in white and the most diverse residues (entropy of 1) in purple.

(E) HIV-1 Env sequence variation around the 2C06 epitope. 2C06 epitope is shown as a blue outline. Part of the 2C06 epitope is highly variable (labeled). The residue at 241 is well conserved with over 96% of isolates having an *N*-linked glycan sequon, whereas BG505 has a glycan hole. See also Figure S3 and Tables S1–S3.



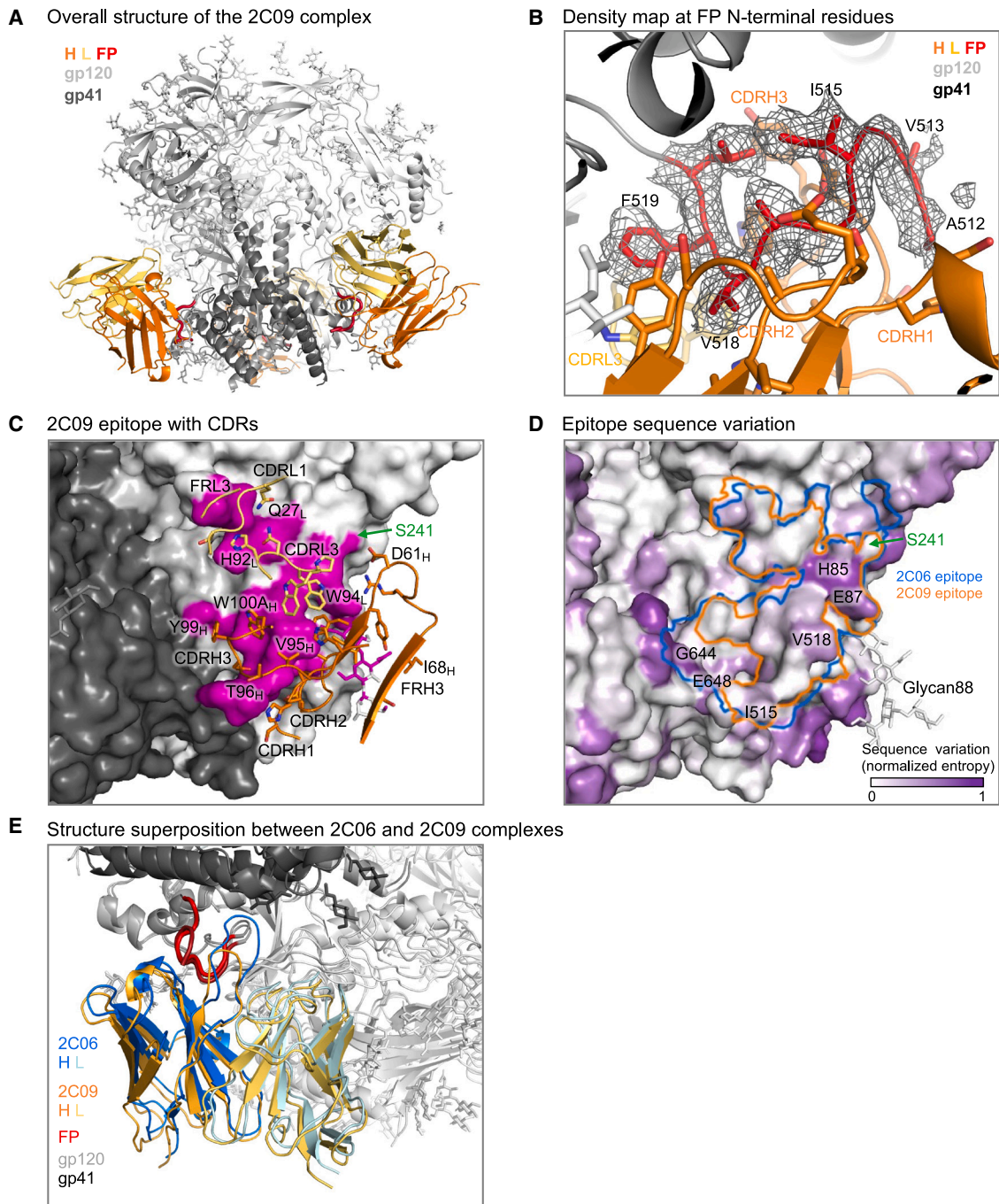


**Figure 3. Cryo-EM structure of N751-2C09.01 in complex with BG505 DS-SOSIP reveals epitope similarity to N751-2C06.01**

(A) Cartoon representation of 2C09 Fab in complex with BG505 DS-SOSIP. 2C09 bound at the fusion-peptide site and interacted with fusion peptide extensively. Heavy chain (H) is shown in orange, light chain (L) in yellow-orange, fusion peptide (FP) in red, the rest of gp41 in darker gray, and gp120 in lighter gray.

(B) Density map showing well-ordered density for fusion peptide. The structure is shown in cartoon representation, with side chains of fusion-peptide residues 512–520 shown in sticks. Some side chains of the antibody interacting with fusion peptide are also shown in sticks.

(C) Epitope details of antibody 2C09 shown for one of the binding sites on the trimer. Env trimer is shown as surface, with subunits in different shades of gray and the epitope surface in magenta. Antibody CDRs and FRs involved in binding are shown in cartoon representation, with interacting side chains shown in sticks. The glycan hole at S241 is on the edge of the epitope and is labeled.

(D) Sequence conservation around the 2C09 epitope. Normalized sequence entropy of HIV-1 group M is mapped on the trimer surface, with absolutely conserved residues (entropy of 0) in white and the most diverse residues (entropy of 1) in purple. 2C09 epitope is shown as an orange outline. The outline of 2C06 is shown in blue for comparison.

(legend continued on next page)

low levels of somatic hypermutation (1% and 3%, respectively, based on nucleotide sequence) (Figures 4A and 4B).

To confirm whether 2C06 and 2C09 were members of the same antibody class, we swapped the heavy and light chains of the two antibodies, as such swapping has in the past confirmed class membership.<sup>27–29</sup> The chimeric antibodies expressed well in mammalian cells and could be purified like the parental 2C06 and 2C09 antibodies. Bio-layer interferometry (BLI) analysis showed that the chimeras could bind BG505 DS-SOSIP and base-covered BG505, similar to 2C06 and 2C09 (Figure 4D). Informatics analysis of the structures revealed that 2C06 and 2C09 shared a heavy-chain variable motif consisting of A<sup>33</sup>XH (superscript number indicates the residue number for a multiple residue motif) and Y58 and a light-chain variable motif consisting of [NH]<sup>92</sup>XW for fusion-peptide binding, and these sequence motifs were compatible with multiple heavy-chain variable genes and several light-chain variable genes (Figure 4E). We used OLGA to calculate the precursor frequency for 2C06 and 2C09 (Figure 4F), finding a frequency of about  $\sim 1$  in 232,000, which is higher than the estimated VRC01 class-antibody precursor frequency.<sup>28</sup> Collectively, these results indicated that 2C06 and 2C09 formed a reproducible antibody class, and we provide details of the expected frequency of this class.

#### Antibody 2C06 partially accommodates, but antibody 2C09 clashes with, glycan241

We next investigated the parameters governing breadth of recognition by antibodies 2C06 and 2C09. As described in the aforementioned structural analysis, both 2C06 and 2C09 epitopes involved S241, a rare glycan hole in BG505 among HIV isolates; specifically, in both 2C06 and 2C09, heavy-chain residues D61 and R64 were within 4–5 Å from S241 side chain, and PISA analysis indicated both 2C06 and 2C09 to bury 14–22 Å<sup>2</sup> surface area with S241 (Table S4). However, the extent that the presence of a glycan at residue 241 might impact recognition was unclear from this analysis.

We therefore created an S241N mutant of glycan-base BG505 (glycan-base BG505-N241), which introduced *N*-linked glycan at position 241, and assessed binding by BLI to 2C06 and 2C09. We observed that presence of glycan241 substantially reduced the binding of 2C09 (to a level similar to the non-neutralizing motavizumab control), whereas 2C06 retained over half of its binding (Figure 5A). Binding to ConC Env trimer, which contains glycan241, was negligible for both 2C06 and 2C09. In comparison, antibody VRC34.01 bound strongly to BG505 DS-SOSIP, ConC, glycan-base BG505, and glycan-base BG505-N241. Other broadly neutralizing fusion-peptide-directed antibodies, vFP16.02 and 0PV-c.01,<sup>17,30</sup> also retained a similar level of binding in the presence of glycan241. By contrast, the narrow-breadth antibodies, A12V163-a.01 and A12V163-b.01 elicited by trimer-only immunization in non-human primates,<sup>17</sup> exhibited about half the reduction in binding in the presence of glycan241, similar to that observed for 2C06. Overall, the results indicated

that binding by antibody 2C06 could partially accommodate the presence of a glycan at position 241, whereas antibody 2C09 clashed with glycan241.

To understand the roles of glycan241 in the recognition of Env trimers by antibodies, we compared the known structures of fusion-peptide-directed antibodies in complex with Env trimers. Except for PGT151,<sup>31</sup> which bound at a site next to glycan611 and glycan637, most fusion-peptide-directed antibodies bound at a similar location, interacting favorably with glycan88 but variably with glycan241 (Figure S5). ACS202 and VRC34.01, both in complex with AMC011 Env,<sup>32</sup> which contains glycan241, interacted favorably with both glycan88 and glycan241 (Figures 5B and S5B). The glycan241 conformations in these two structures are similar. In fact, alignment of all Env-trimer structures from the Protein Data Bank (PDB) with two or more sugar residues built for glycan241 revealed all glycan241 conformations to be similar (Figure 5C), suggesting this conformation to be the most energetically favorable. When this glycan241 conformation was superimposed on the structures of 2C06 and 2C09, however, steric clashes were observed (Figure 5D), although another glycan241 conformation could be modeled that avoided clashes with 2C06 and 2C09 (Figure 5D). We note that neutralizing antibodies vFP16.02, 0PV-c.01, A12V163-a.01, and A12V163-b.01 all showed substantial clashes with glycan241 in the conformation defined by antibody-ACS202 complexes (Figure 5E). The broadly neutralizing antibodies vFP16.02 and 0PV-c.01 likely accommodate the presence of 241, as they neutralize strains that have a glycan at this position; however, the strain-specific antibodies A12V163-a.01 and A12V163-b.01—although they retain at least one-third of their affinity to BG505-241—were incapable of neutralizing any strains with glycan241, suggesting that these antibodies, like 2C06 and 2C09, have their neutralization substantially impacted by glycan241. Notably, introduction of *N*-linked glycan at 241 in BG505 pseudovirus resulted in the loss of neutralization by both 2C06 and 2C09 (Figure S2E), confirming the importance of this glycan hole in the recognition of these two antibodies.

#### High-entropy epitope residues contribute to the strain specificity of 2C06 and 2C09

While recognition of the 241 glycan hole explains much of the strain specificity of 2C06 and 2C09, there were seven strains other than BG505 in our 208-isolate panel missing glycan241, and we next investigated whether HIV sequence diversity of the epitope residues contributed to the strain-specific neutralization of these antibodies.

We calculated the BSA-weighted average entropy of the epitope residues for fusion-peptide-directed antibodies as well as other broad HIV-neutralizing antibodies. We observed a negative correlation between epitope entropy and neutralization breadth for non-fusion peptide HIV-neutralizing antibodies (Figure 6A and Table S2). However, antibodies binding at the fusion-peptide site of vulnerability all had very similar normalized

(E) Structure superposition between 2C06 and 2C09 complexes. The two structures were aligned by the gp41 subunit bearing the fusion peptide shown. The fusion peptide in both structures were in similar conformation except the first two residues, which in 2C09 (darker red) folded back down to interact with the antibody and in 2C06 extended up to bind the C-terminal helix of neighboring gp41 (top left). See also Figure S4 and Tables S1–S3.





epitope entropies of 0.24–0.30, except for PGT151, which bound to a slightly different region from other fusion-peptide-directed antibodies (Figure S5). This finding suggested that the strain specificity for fusion-peptide-directed antibodies was unrelated to overall epitope entropy but instead related to an inability to accommodate the variation that is intrinsically inherent to the fusion-peptide site of vulnerability.

To identify epitope residues in BG505 that contribute to strain specificity, we analyzed Shannon entropy and BSA of epitope residues of 2C06 and 2C09 (Figure 6B). Fusion-peptide residues were well conserved among HIV isolates except at positions 515 and 518, with normalized entropy above 0.4 (Figure S6A). Outside of the fusion peptide itself, however, there were several residues in 2C06 or 2C09 epitopes with high entropy (Figure 6B). Of these, position 85 had a normalized entropy of 0.733, and in BG505 this position was a histidine, which had a frequency of 2.5% among HIV-1 group M isolates; and position 644 was a glycine in BG505, which had 1.7% frequency and a normalized entropy of 0.729. H85 had similar tight interactions with both 2C06 and 2C09, surrounded by side chains from CDR H2 (Y47 and Y58), FR H3 (D61 and R64), CDR L3 (W94 and P95), and light-chain N-terminal residue E1 (Figures 6C and S6B). The presence of the most frequent residue valine at this position would likely clash with CDR L3, which also played a role in binding fusion peptide (Figure 6C). In terms of neutralization, of the eight strains in our 208-strain panel lacking glycan241, there were two strains with histidine at 85, T257-31 and CNE56, in addition to BG505; both 2C06 and 2C09 could not neutralize these two strains (Figure S2E). Residue G644 in the 2C06 complex had tight interactions with R100A side chain of CDR H3, which played an important role in binding fusion peptide. Mutation of G644 to other amino acids would clash with arginine at residue position 100A, contributing to the strain-specific neutralization of 2C06 (Figure 6D). In terms of neutralization, other than BG505, none of the other strains lacking a glycan at 241 had G644, so 2C06 would be unlikely to neutralize these. 2C09 does not interact with position 644 and might have a chance to neutralize some of them. However, experimental assessment of neutralization indicated that neither 2C06 nor 2C09 could neutralize any of the other strains lacking a glycan at 241 in our 208-strain panel (Figure S2E).

To confirm the observed interactions of the epitope residues with substantial entropy, we mutated H85 or G644 in BG505 DS-SOSIP to the more frequent utilized amino acids among HIV-1 isolates and assessed the mutants for binding to 2C06 and 2C09 (Figure S6D). Mutation of H85 to valine, the most frequent amino acid, reduced the binding to both antibodies by half, whereas mutation to glutamate, the second most frequent, reduced binding by more than 6-fold. Mutation of G644 to arginine (the most frequent) or threonine (the second most frequent) reduced binding to 2C06 by more than 5-fold, but reduced 2C09 binding by about half. These results confirmed the role of H85 and G644 in antibody binding as observed in structures.

Overall, the above analyses suggested that fusion-peptide-directed neutralizing antibodies elicited by BG505 Env immunization can partially accommodate the glycan hole at position 241. Those that do, however, encounter other BG505 strain-specific residues, proximal to fusion peptide, and their inability to accommodate variation at these other positions contributes to their strain specificity.

## DISCUSSION

As noted above, the HIV Env trimer evades antibody-mediated neutralization by conformational masking, glycan shielding, and sequence variation. Env trimers stabilized in the prefusion-closed conformation, however, induce recognition of the neutralization-susceptible shape of Env, and their use in human vaccine trials such as VRC 018<sup>22</sup> enables insight into how the two remaining mechanisms of Env evasion, glycan shielding and sequence variation, impact the induction of neutralizing responses. Here, we observed glycan shielding to reduce immunogenicity of most of the Env surface such that ~90% of Env-trimer reactive B cells were directed at the protein-exposed base of the trimer, and—for those antibodies that recognized other regions on the trimer—only ~1% bound with sufficient affinity to neutralize (Figure 1). In terms of sequence variation, the few elicited neutralizing antibodies showed partial recognition of strain-specific glycan holes, such as at glycan241 on BG505 (Figures 2, 3, 4, and 5), and these antibodies were generally incapable of accommodating sequence variation even at the moderate level (epitope entropies of 0.24–0.30) that appeared to be present in antibodies that target the fusion-peptide site of vulnerability (Figure 6). Thus, partial recognition of a BG505-specific glycan hole and binding requirements for a few BG505-specific residues combined to make antibodies 2C06 and 2C09 highly specific for strain BG505.

We previously observed in the VRC 018 clinical trial<sup>22</sup> that some participants showed detectable neutralization against BG505.N611Q, a mutant BG505 strain with glycan611 removed that is >10-fold more sensitive to fusion-peptide-directed antibodies than wild-type BG505.<sup>8</sup> This, along with the observation in the current study that the initially identified neutralizing antibodies from humans vaccinated with BG505 DS-SOSIP trimer were fusion-peptide directed, suggested that strain BG505 might be especially good at eliciting fusion-peptide-directed antibodies, likely because of the lack of glycan241, which is proximal to the fusion-peptide site of vulnerability, as the presence of a glycan hole increases the elicitation of antibodies targeting proximal epitopes.<sup>33–35</sup>

It will be interesting to see how prefusion-stabilized Env-trimer immunization can be altered to overcome glycan shielding and sequence variation. One way to overcome immunogenicity issues related to glycan shielding might be to mask the exposed protein base on the trimer with *N*-linked glycans<sup>36</sup> or by using membrane-bound trimers, such as those delivered by

(D) Binding analysis of chimeras swapping heavy and light chains between 2C06 and 2C09. Data were measured once.

(E) Sequence signatures of the reproducible 2C06 and 2C09 class for fusion-peptide binding. HV, heavy-chain variable; LV, light-chain variable. See also Table S6.

(F) Calculated precursor frequency of 2C06/2C09 antibody class for healthy donors HIP1–HIP3 (see STAR Methods).

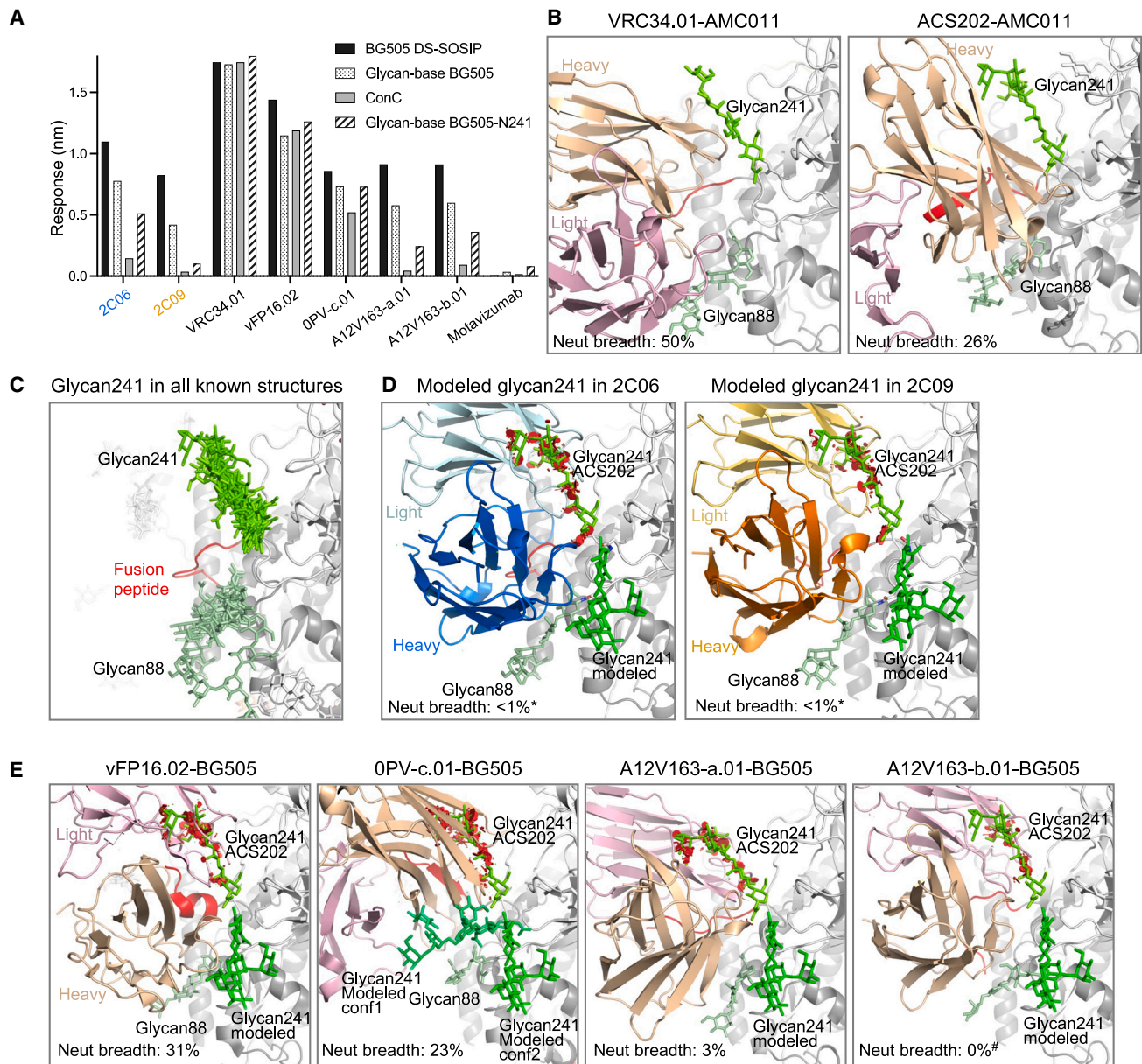


**Figure 5. Antibody 2C06 partially accommodates, but antibody 2C09 clashes with, glycan241**

(A) BLI binding analysis of 2C06 and 2C09 with Env trimers with or without glycan241 in comparison with other fusion-peptide-directed antibodies. Both BG505 DS-SOSIP and glycan-base BG505 have serine at 241. Glycan-base BG505-N241 is an S241N mutant of glycan-base BG505 containing *N*-glycosylation sequon at 241. ConC harbors glycan241. Motavizumab is a negative control. Data were measured once.

(B) Structures of VRC34.01 (PDB: 6nc3) and ACS202 (PDB: 6nc2), both in complex with AMC011 Env, which contains glycan241, reveal that both antibodies interact favorably with glycan88 and glycan241, shown in different shades of green. Neutralization breadths were for half-maximal inhibitory concentration ( $IC_{50}$ ) < 50  $\mu$ g/mL in the 208-strain panel.

(C) Structural alignment of Env trimers from the PDB with two or more sugar residues built for glycan241. The structures were aligned by the gp120 subunit bearing the glycan241 shown. Antibodies, if present in the structure, are not shown for clarity. Glycan88 and glycan241 are shown in different shades of green, with the same view as in other structural panels of the figure. PDB: 6olp, 6vo3, 7rsn, 7rso, 6ohy, 7n6u, 6vrw, 6myy, 7llk, 6u59, 5vn8, 6p65, 6vy2, 7lua, 6okp, 7l6o, 6nc3, 6nc2.

(D) Antibodies 2C06 and 2C09 clash with the glycan241 conformation seen in all known Env structures containing glycan241. The structures were aligned with that of ACS202-AMC011 complex by the gp120 subunit bearing the glycan241 shown. Clashes between antibody 2C06 or 2C09 and glycan241 in the ACS202 complex are shown as red disks in PyMOL (<https://pymol.org/2/>). A different glycan conformation could be modeled (shown in bright green) that did not clash with the antibody. Asterisks denote that 2C06 and 2C09 neutralize BG505 only.

(legend continued on next page)



liposomes<sup>37,38</sup> or on virus-like particles.<sup>39</sup> In terms of sequence variation, immunization with diverse trimers appears to be one way to avoid or to mature responses to strain-specific glycan holes. These strategies can be combined with epitope focusing such as by removal of glycans proximal to the CD4-binding site<sup>34,40</sup> or by induction of antibodies against a conserved portion of an epitope, such as by first priming with the N terminus of the fusion peptide to create an antigenic hotspot.<sup>17</sup> More recent results with non-human primates suggest that appropriate maturation of the immune response to the prefusion-stabilized Env trimers might be critical, with broadly neutralizing responses observed even after immunization with only a single Env trimer.<sup>19</sup> It will be fascinating to determine the molecular characteristics of elicited neutralizing antibodies from this recent non-human primate study and to find out how they differ from those described here from Env-trimer immunization of humans.

### Limitations of the study

This study describes antibodies isolated from a single donor at a single time point. The quality of isolated antibodies is also limited by the source of the study, the VRC 018 clinical trial, which was designed for the primary goal of testing the safety of BG505 DS-SOSIP adjuvanted by alum as a vaccine candidate. As a result, the antibodies isolated have limited somatic hypermutations and low neutralization potency with strain specificity.

### STAR★METHODS

Detailed methods are provided in the online version of this paper and include the following:

- **KEY RESOURCES TABLE**
- **RESOURCE AVAILABILITY**
  - Lead contact
  - Materials availability
  - Data and code availability
- **EXPERIMENTAL MODEL AND SUBJECT DETAILS**
  - Serum samples
  - Cell lines
- **METHOD DETAILS**
  - Preparation of Env trimers and antigen-specific probes
  - B cell sorting
  - Rapid assembly, transfection, and production of immunoglobulins (RATP-Ig)
  - AlphaLISA screening of RATP-Ig supernatants
  - Antibody preparation
  - Env-pseudovirus neutralization assays
  - Enzyme-linked immunosorbent assay (ELISA)
  - IgG binding affinity measured by Carterra
  - Bio-layer interferometry (BLI)
  - Surface plasmon resonance measurements of Fab binding affinity

- Cryo-EM sample preparation and data collection
- Model building and refinement
- Antibody recombination and sequence signature analyses
- **QUANTIFICATION AND STATISTICAL ANALYSIS**

### SUPPLEMENTAL INFORMATION

Supplemental information can be found online at <https://doi.org/10.1016/j.celrep.2023.112755>.

### ACKNOWLEDGMENTS

We thank Jonathan Stuckey for assistance with figures, members of the Virology Laboratory and Vector Core, Vaccine Research Center, for discussions and comments on the manuscript, and David Ho and members of the Aaron Diamond AIDS Research Center for helpful comments. We thank Preeti Apte, Anita Arthur, Allison Beck, Nina Berkowitz, Pamela Costner, Jennifer Cunningham, Aba Eshun, Ingelise J. Gordon, Cynthia S. Hendel, Renunda Hicks, LaSonji Holman, Katherine Houser, Brenda Larkin, Floreliz Mendoza, Abidemi Ola, Karen Parker, Sarah Plummer, Ro Shauna Rothwell, Jamie Saunders, Olga Trofymenko, Xiaolin Wang, William Whalen, and Alicia T. Widge of the VRC 018 clinical trial team for providing the human PMBC samples. We thank the VRC Production Program for providing ConC and BG505 Env trimers; the VRP Production Program includes Nadia Amharref, Frank J. Arnold, Nathan Barefoot, Christopher Barry, Elizabeth Carey, Ria Caringal, Kevin Carlton, Naga Chalamalsetty, Adam Charlton, Rajoshi Chaudhuri, Mingzhong Chen, Peifeng Chen, Yue Chen, Nicole Cibelli, Jonathan W. Cooper, Hussain Dahodwala, Marianna Fleischman, Julia C. Frederick, Haley C. Fuller, Jason G. Gall, Isaac Godfroy, Deepika Gollapudi, Daniel Gowetski, Krishana Gulla, Joe Horwitz, Althaf Hussain, Vera Ivleva, Tina Khin, Lisa Kuelzto, Gabriella Lagos, Q. Paula Lei, Yile Li, Venkata Mangalampalli, Gabriel Moxey, Sarah O'Connell, Aakash Patel, Erwin Rosales-Zavala, Elizabeth Scheideman, Nicole A. Schneck, Zachary Schneiderman, Andrew Shaddeau, William Shadrick, Shamitha Shetty, Brad Tippet, Alison Vinitzky, Calvin Webber, Sara Witter, Lu Yang, Yanhong Yang, and Yaqiu Zhang. This study used the Office of Cyber Infrastructure and Computational Biology High Performance Computing cluster at the National Institute of Allergy and Infectious Diseases, Bethesda, MD. Support for this work was provided by the Intramural Research Program of the Vaccine Research Center, National Institute of Allergy and Infectious Diseases, National Institutes of Health. Part of the cryo-EM data collection was performed at the Columbia University Cryo-Electron Microscopy Center, which was funded in part by the Frederick National Laboratory for Cancer Research, NIH, under contract HHSN261200800001.

### AUTHOR CONTRIBUTIONS

S.W. determined cryo-EM structures, analyzed the data, and wrote the manuscript; F.M. performed B cell sorting; B.Z. and T.L. expressed and purified antibodies and performed BLI assays; C.-H.S. analyzed antibody sequences and binding motifs; T.B. calculated Shannon entropy from the 208-strain panel and analyzed fusion-peptide-directed antibodies for epitope overlaps; T.J., A.R.H., and J.R.-T. carried out RATP-Ig for the sorted B cells; I.-T.T. and D.W. produced trimer probes; P.T. performed AlphaLISA and Carterra assays; J.E.B. and N.C.M. collected cryo-EM data for 2C06; A.C. provided BG505 DS-SOSIP and ConC trimers; R.C. and A.S.O. prepared BG505 DS-SOSIP mutants and analyzed for antibody binding by BLI; C.C. and D.K.P. performed ELISA; M.G. and L.N. provided serum samples from VRC 018 trial; J.G., R.R., and A.S.O. designed glycan-base BG505; D.R.H. and A.S.O. produced

(E) Antibodies derived from mouse immunizations, vFP16.02 (PDB: 6cdi), and from non-human primates, OPV-c.01 (PDB: 6nf2), A12V163-a.01 (PDB: 6n1v), and A12V163-b.01 (PDB: 6mgp), all of which clash with the glycan241 conformation in ACS202. A different glycan241 conformation, similar to that for 2C06 and 2C09, could be modeled, which avoids any clashes. Binding of OPV-c.01 allows for more space for multiple conformations of modeled glycan241. Hash mark denotes that A12V163-b.01 neutralizes only at IC<sub>50</sub> > 50 μg/mL.

See also [Figures S2](#) and [S5](#); [Table S4](#).



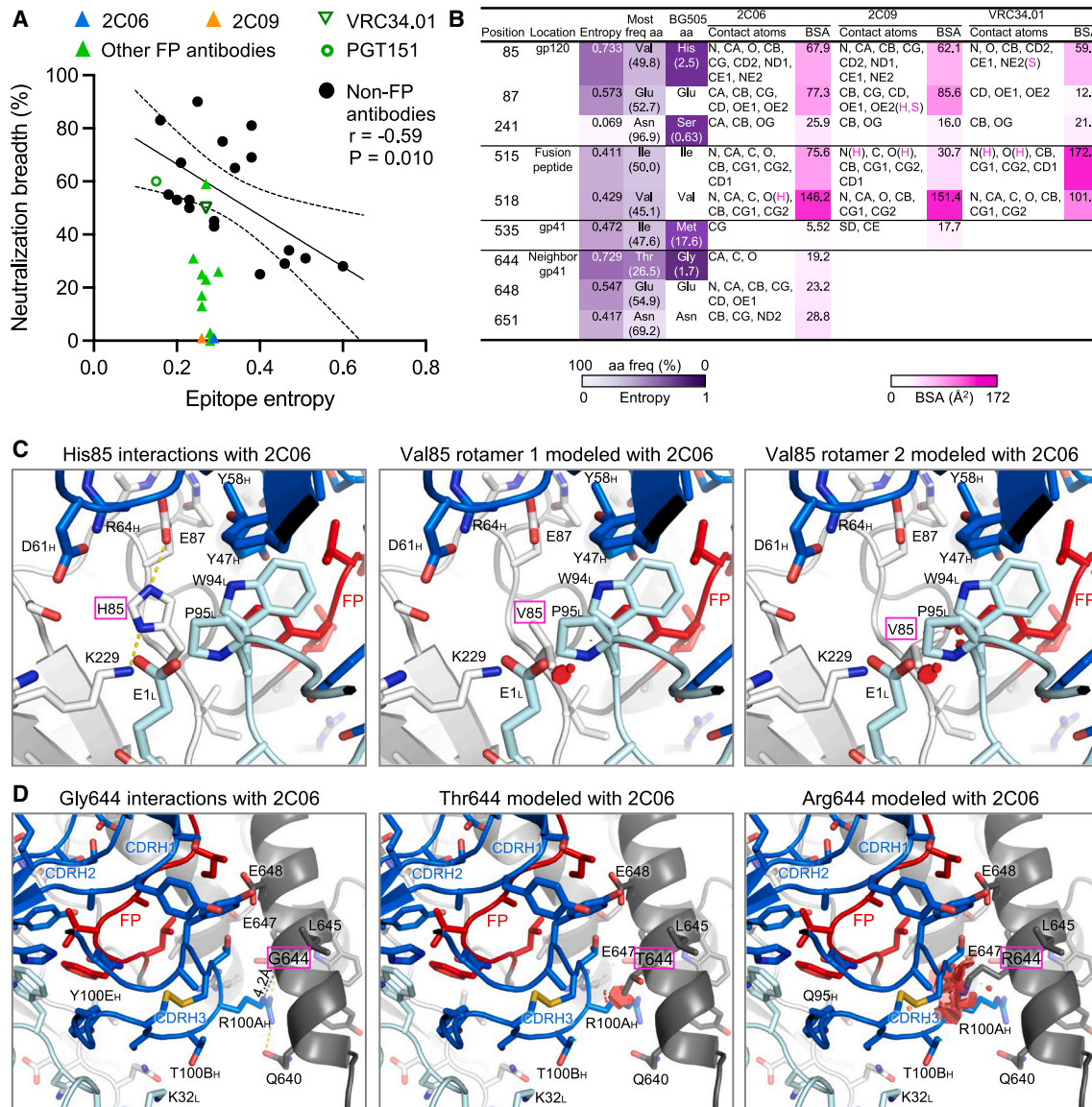


**Figure 6. Recognition requirements for high-entropy residues contribute to strain specificity of 2C06 and 2C09**

(A) While neutralization breadth generally correlates with epitope entropy, antibodies directed to the fusion-peptide sites of vulnerability have similar epitope entropy. Neutralization breadth represents the percentage of the 208-strain panel neutralized with  $IC_{50} < 50 \mu\text{g/mL}$ . Epitope entropy was calculated as BSA-weighted average of normalized Shannon's entropy on the Env sequences of the 208-strain panel.

(B) Analyses of sequence entropy and contact surface areas of residues in strain-specific and broadly neutralizing fusion-peptide-directed antibodies. Epitope residues with normalized entropy above 0.4 are listed, as well as residue S241, which has low entropy but with low frequency as serine among HIV-1 isolates. The contact atoms and areas for VRC34.01 were calculated from PDB: 5i8h (VRC34.01 also binds AMC011 Env, which has valine85). Entropy values were calculated with Shannon Entropy-One ([https://www.hiv.lanl.gov/content/sequence/ENTROPY/entropy\\_one.html](https://www.hiv.lanl.gov/content/sequence/ENTROPY/entropy_one.html)) on the curated alignment of year 2020 HIV-1 M group Env of 5,255 sequences (<https://www.hiv.lanl.gov/content/sequence/NEWALIGN/align.html>), and were normalized to have values between 0 and 1. Contact atoms and BSA were calculated with PISA ([https://www.ebi.ac.uk/msd-srv/prot\\_int/cgi-bin/piserver](https://www.ebi.ac.uk/msd-srv/prot_int/cgi-bin/piserver)). Hydrogen bonds or salt bridges involved with the contact atoms are designated as H or S, respectively.

(C) H85, with high Shannon entropy of 0.733 and 2.5% frequency, has tight interactions with antibody heavy- and light-chain residues in both structures of the 2C06 complex (2C09 has nearly identical interactions, see Figure S6). Modeling in PyMOL with the most frequent amino acid valine results in clashes with CDR L3, either P95 or W94 or both, with any rotamers. The second most common amino acid at 85 is glutamate at 8.5% frequency and would have severe clashes with the antibody. (D) Antibody 2C06 had close contact with G644 from its R100A side chain of CDR H3, which played a major role in binding fusion peptide. Modeling as threonine (26.5% frequency) or arginine (20.1%) would result in clashes, disrupting CDR H3 interactions with fusion peptide.

See also Figures S2 and S6.

trimers for binding analysis; M.L. modeled glycan241 conformation and calculated energies for epitope residue mutations; S.O. and N.A.D.-R. performed neutralization assays; T.S. and Y.T. collected cryo-EM data for 2C09; D.J.V.W. and T.Z. performed SPR assays; R.A.K. oversaw neutralization and ELISA experiments; L.S. supervised data collection for 2C06; D.C.D. supervised RATP-Ig experiments; A.B.M. supervised B cell sorting; P.D.K. oversaw the project and—with S.W.—wrote the manuscript, with all authors providing revisions and comments.

#### DECLARATION OF INTERESTS

The authors declare no competing interests.

Received: February 26, 2023

Revised: April 18, 2023

Accepted: June 21, 2023

Published: July 11, 2023

#### REFERENCES

- Kwong, P.D., DeKosky, B.J., and Ulmer, J.B. (2020). Antibody-guided structure-based vaccines. *Semin. Immunol.* 50, 101428. <https://doi.org/10.1016/j.smm.2020.101428>.
- Wei, X., Decker, J.M., Wang, S., Hui, H., Kappes, J.C., Wu, X., Salazar-Gonzalez, J.F., Salazar, M.G., Kilby, J.M., Saag, M.S., et al. (2003). Antibody neutralization and escape by HIV-1. *Nature* 422, 307–312. <https://doi.org/10.1038/nature01470>.
- Starcich, B.R., Hahn, B.H., Shaw, G.M., McNeely, P.D., Modrow, S., Wolf, H., Parks, E.S., Parks, W.P., Josephs, S.F., Gallo, R.C., et al. (1986). Identification and characterization of conserved and variable regions in the envelope gene of HTLV-III/LAV, the retrovirus of AIDS. *Cell* 45, 637–648.
- Robert-Guroff, M., Brown, M., and Gallo, R.C. (1985). HTLV-III-neutralizing antibodies in patients with AIDS and AIDS-related complex. *Nature* 316, 72–74. <https://doi.org/10.1038/316072a0>.
- Weiss, R.A., Clapham, P.R., Cheingsong-Popov, R., Dalgleish, A.G., Carne, C.A., Weller, I.V., and Tedder, R.S. (1985). Neutralization of human T-lymphotropic virus type III by sera of AIDS and AIDS-risk patients. *Nature* 316, 69–72. <https://doi.org/10.1038/316069a0>.
- Wu, X., Zhou, T., Zhu, J., Zhang, B., Georgiev, I., Wang, C., Chen, X., Longo, N.S., Louder, M., McKee, K., et al. (2011). Focused evolution of HIV-1 neutralizing antibodies revealed by structures and deep sequencing. *Science* 333, 1593–1602. <https://doi.org/10.1126/science.1207532>.
- Huang, J., Ofek, G., Laub, L., Louder, M.K., Doria-Rose, N.A., Longo, N.S., Imamichi, H., Bailer, R.T., Chakrabarti, B., Sharma, S.K., et al. (2012). Broad and potent neutralization of HIV-1 by a gp41-specific human antibody. *Nature* 491, 406–412. <https://doi.org/10.1038/nature11544>.
- Kong, R., Xu, K., Zhou, T., Acharya, P., Lemmin, T., Liu, K., Ozorowski, G., Soto, C., Taft, J.D., Bailer, R.T., et al. (2016). Fusion peptide of HIV-1 as a site of vulnerability to neutralizing antibody. *Science* 352, 828–833. <https://doi.org/10.1126/science.aae0474>.
- Doria-Rose, N.A., Bhiman, J.N., Roark, R.S., Schramm, C.A., Gorman, J., Chuang, G.Y., Pancera, M., Cale, E.M., Ernandes, M.J., Louder, M.K., et al. (2016). New Member of the V1V2-Directed CAP256-VRC26 Lineage That Shows Increased Breadth and Exceptional Potency. *J. Virol.* 90, 76–91. <https://doi.org/10.1128/JVI.01791-15>.
- Walker, L.M., Huber, M., Doores, K.J., Falkowska, E., Pejchal, R., Julien, J.P., Wang, S.K., Ramos, A., Chan-Hui, P.Y., Moyle, M., et al. (2011). Broad neutralization coverage of HIV by multiple highly potent antibodies. *Nature* 477, 466–470. <https://doi.org/10.1038/nature10373>.
- Hraber, P., Seaman, M.S., Bailer, R.T., Mascola, J.R., Montefiori, D.C., and Korber, B.T. (2014). Prevalence of broadly neutralizing antibody responses during chronic HIV-1 infection. *AIDS* 28, 163–169. <https://doi.org/10.1097/QAD.000000000000106>.
- Walker, L.M., Phogat, S.K., Chan-Hui, P.Y., Wagner, D., Phung, P., Goss, J.L., Wrin, T., Simek, M.D., Fling, S., Mitcham, J.L., et al. (2009). Broad and potent neutralizing antibodies from an African donor reveal a new HIV-1 vaccine target. *Science* 326, 285–289. <https://doi.org/10.1126/science.1178746>.
- Sanders, R.W., Derking, R., Cupo, A., Julien, J.P., Yasmeen, A., de Val, N., Kim, H.J., Blattner, C., de la Peña, A.T., Korzun, J., et al. (2013). A next-generation cleaved, soluble HIV-1 Env trimer, BG505 SOSIP.664 gp140, expresses multiple epitopes for broadly neutralizing but not non-neutralizing antibodies. *PLoS Pathog.* 9, e1003618. <https://doi.org/10.1371/journal.ppat.1003618>.
- de Taeye, S.W., Ozorowski, G., Torrents de la Peña, A., Guttman, M., Julien, J.P., van den Kerkhof, T.L.G.M., Burger, J.A., Pritchard, L.K., Pugach, P., Yasmeen, A., et al. (2015). Immunogenicity of Stabilized HIV-1 Envelope Trimers with Reduced Exposure of Non-neutralizing Epitopes. *Cell* 163, 1702–1715. <https://doi.org/10.1016/j.cell.2015.11.056>.
- Klasse, P.J., LaBranche, C.C., Ketas, T.J., Ozorowski, G., Cupo, A., Pugach, P., Ringe, R.P., Golabek, M., van Gils, M.J., Guttman, M., et al. (2016). Sequential and Simultaneous Immunization of Rabbits with HIV-1 Envelope Glycoprotein SOSIP.664 Trimers from Clades A, B and C. *PLoS Pathog.* 12, e1005864. <https://doi.org/10.1371/journal.ppat.1005864>.
- McCoy, L.E., van Gils, M.J., Ozorowski, G., Messmer, T., Briney, B., Voss, J.E., Kulp, D.W., Macauley, M.S., Sok, D., Pauthner, M., et al. (2016). Holes in the Glycan Shield of the Native HIV Envelope Are a Target of Trimer-Elicited Neutralizing Antibodies. *Cell Rep.* 16, 2327–2338. <https://doi.org/10.1016/j.celrep.2016.07.074>.
- Kong, R., Duan, H., Sheng, Z., Xu, K., Acharya, P., Chen, X., Cheng, C., Dingens, A.S., Gorman, J., Sastry, M., et al. (2019). Antibody Lineages with Vaccine-Induced Antigen-Binding Hotspots Develop Broad HIV Neutralization. *Cell* 178, 567–584.e19. <https://doi.org/10.1016/j.cell.2019.06.030>.
- Saunders, K.O., Edwards, R.J., Tilahun, K., Manne, K., Lu, X., Cain, D.W., Wiehe, K., Williams, W.B., Mansouri, K., Hernandez, G.E., et al. (2022). Stabilized HIV-1 envelope immunization induces neutralizing antibodies to the CD4bs and protects macaques against mucosal infection. *Sci. Transl. Med.* 14, eabo5598. <https://doi.org/10.1126/scitranslmed.abo5598>.
- Lee, J.H., Sutton, H.J., Cottrell, C.A., Phung, I., Ozorowski, G., Sewall, L.M., Nedellec, R., Nakao, C., Silva, M., Richey, S.T., et al. (2022). Long-primed germinal centres with enduring affinity maturation and clonal migration. *Nature* 609, 998–1004. <https://doi.org/10.1038/s41586-022-05216-9>.
- Kwon, Y.D., Pancera, M., Acharya, P., Georgiev, I.S., Crooks, E.T., Gorman, J., Joyce, M.G., Guttman, M., Ma, X., Narpala, S., et al. (2015). Crystal structure, conformational fixation and entry-related interactions of mature ligand-free HIV-1 Env. *Nat. Struct. Mol. Biol.* 22, 522–531. <https://doi.org/10.1038/nsmb.3051>.
- Gulla, K., Cibelli, N., Cooper, J.W., Fuller, H.C., Schneiderman, Z., Witter, S., Zhang, Y., Changela, A., Geng, H., Hatcher, C., et al. (2021). A non-affinity purification process for GMP production of prefusion-closed HIV-1 envelope trimers from clades A and C for clinical evaluation. *Vaccine* 39, 3379–3387. <https://doi.org/10.1016/j.vaccine.2021.04.063>.
- Houser, K.V., Gaudinski, M.R., Happe, M., Narpala, S., Verardi, R., Sarfo, E.K., Corrigan, A.R., Wu, R., Rothwell, R.S., Novik, L., et al. (2022). Safety and immunogenicity of an HIV-1 prefusion-stabilized envelope trimer (Trimer 4571) vaccine in healthy adults: A first-in-human open-label, randomized, dose-escalation, phase 1 clinical trial. *EClinicalMedicine* 48, 101477. <https://doi.org/10.1016/j.eclim.2022.101477>.
- Chuang, G.Y., Lai, Y.T., Boyington, J.C., Cheng, C., Geng, H., Narpala, S., Rawi, R., Schmidt, S.D., Tsybovsky, Y., Verardi, R., et al. (2020). Development of a 3Mut-Apex-Stabilized Envelope Trimer That Expands HIV-1 Neutralization Breadth When Used To Boost Fusion Peptide-Directed Vaccine-Elicited Responses. *J. Virol.* 94, e00074-20. <https://doi.org/10.1128/JVI.00074-20>.
- Cheng, C., Xu, K., Kong, R., Chuang, G.Y., Corrigan, A.R., Geng, H., Hill, K.R., Jafari, A.J., O'Dell, S., Ou, L., et al. (2019). Consistent elicitation of

- cross-clade HIV-neutralizing responses achieved in guinea pigs after fusion peptide priming by repetitive envelope trimer boosting. *PLoS One* 14, e0215163. <https://doi.org/10.1371/journal.pone.0215163>.
25. Lima, N.S., Musayev, M., Johnston, T.S., Wagner, D.A., Henry, A.R., Wang, L., Yang, E.S., Zhang, Y., Birungi, K., Black, W.P., et al. (2022). Primary exposure to SARS-CoV-2 variants elicits convergent epitope specificities, immunoglobulin V gene usage and public B cell clones. *Nat. Commun.* 13, 7733. <https://doi.org/10.1038/s41467-022-35456-2>.
  26. Chuang, G.Y., Zhou, J., Acharya, P., Rawi, R., Shen, C.H., Sheng, Z., Zhang, B., Zhou, T., Bailer, R.T., Dandey, V.P., et al. (2019). Structural Survey of Broadly Neutralizing Antibodies Targeting the HIV-1 Env Trimer Delineates Epitope Categories and Characteristics of Recognition. *Structure* 27, 196–206.e6. <https://doi.org/10.1016/j.str.2018.10.007>.
  27. Jardine, J.G., Ota, T., Sok, D., Pauthner, M., Kulp, D.W., Kalyuzhnyi, O., Skog, P.D., Thinnis, T.C., Bhullar, D., Briney, B., et al. (2015). HIV-1 VACCINES. Priming a broadly neutralizing antibody response to HIV-1 using a germline-targeting immunogen. *Science* 349, 156–161. <https://doi.org/10.1126/science.aac5894>.
  28. Zhou, T., Zhu, J., Wu, X., Moquin, S., Zhang, B., Acharya, P., Georgiev, I.S., Altae-Tran, H.R., Chuang, G.Y., Joyce, M.G., et al. (2013). Multidonor analysis reveals structural elements, genetic determinants, and maturation pathway for HIV-1 neutralization by VRC01-class antibodies. *Immunity* 39, 245–258. <https://doi.org/10.1016/j.immuni.2013.04.012>.
  29. Zhu, J., Wu, X., Zhang, B., McKee, K., O'Dell, S., Soto, C., Zhou, T., Casazza, J.P., NISC Comparative Sequencing Program, and Mullikin, J.C., et al. (2013). De novo identification of VRC01 class HIV-1-neutralizing antibodies by next-generation sequencing of B-cell transcripts. *Proc. Natl. Acad. Sci. USA* 110, E4088–E4097. <https://doi.org/10.1073/pnas.1306262110>.
  30. Xu, K., Acharya, P., Kong, R., Cheng, C., Chuang, G.Y., Liu, K., Louder, M.K., O'Dell, S., Rawi, R., Sastry, M., et al. (2018). Epitope-based vaccine design yields fusion peptide-directed antibodies that neutralize diverse strains of HIV-1. *Nat. Med.* 24, 857–867. <https://doi.org/10.1038/s41591-018-0042-6>.
  31. Blattner, C., Lee, J.H., Slieden, K., Derking, R., Falkowska, E., de la Peña, A.T., Cupo, A., Julien, J.P., van Gils, M., Lee, P.S., et al. (2014). Structural delineation of a quaternary, cleavage-dependent epitope at the gp41-gp120 interface on intact HIV-1 Env trimers. *Immunity* 40, 669–680. <https://doi.org/10.1016/j.immuni.2014.04.008>.
  32. Yuan, M., Cottrell, C.A., Ozorowski, G., van Gils, M.J., Kumar, S., Wu, N.C., Sarkar, A., Torres, J.L., de Val, N., Copps, J., et al. (2019). Conformational Plasticity in the HIV-1 Fusion Peptide Facilitates Recognition by Broadly Neutralizing Antibodies. *Cell Host Microbe* 25, 873–883.e5. <https://doi.org/10.1016/j.chom.2019.04.011>.
  33. Crooks, E.T., Tong, T., Chakrabarti, B., Narayan, K., Georgiev, I.S., Menis, S., Huang, X., Kulp, D., Osawa, K., Muranaka, J., et al. (2015). Vaccine-Elicited Tier 2 HIV-1 Neutralizing Antibodies Bind to Quaternary Epitopes Involving Glycan-Deficient Patches Proximal to the CD4 Binding Site. *PLoS Pathog.* 11, e1004932. <https://doi.org/10.1371/journal.ppat.1004932>.
  34. Zhou, T., Doria-Rose, N.A., Cheng, C., Stewart-Jones, G.B.E., Chuang, G.Y., Chambers, M., Druz, A., Geng, H., McKee, K., Kwon, Y.D., et al. (2017). Quantification of the Impact of the HIV-1-Glycan Shield on Antibody Elicitation. *Cell Rep.* 19, 719–732. <https://doi.org/10.1016/j.celrep.2017.04.013>.
  35. Lee, M., Changela, A., Gorman, J., Rawi, R., Bylund, T., Chao, C.W., Lin, B.C., Louder, M.K., Ota, A.S., Zhang, B., et al. (2021). Extended antibody-framework-to-antigen distance observed exclusively with broad HIV-1-neutralizing antibodies recognizing glycan-dense surfaces. *Nat. Commun.* 12, 6470. <https://doi.org/10.1038/s41467-021-26579-z>.
  36. Kulp, D.W., Steichen, J.M., Pauthner, M., Hu, X., Schiffner, T., Liguori, A., Cottrell, C.A., Havenar-Daughton, C., Ozorowski, G., Georgeson, E., et al. (2017). Structure-based design of native-like HIV-1 envelope trimers to silence non-neutralizing epitopes and eliminate CD4 binding. *Nat. Commun.* 8, 1655. <https://doi.org/10.1038/s41467-017-01549-6>.
  37. Bale, S., Goebrecht, G., Stano, A., Wilson, R., Ota, T., Tran, K., Ingale, J., Zwick, M.B., and Wyatt, R.T. (2017). Covalent Linkage of HIV-1 Trimers to Synthetic Liposomes Elicits Improved B Cell and Antibody Responses. *J. Virol.* 91, e00443-17. <https://doi.org/10.1128/JVI.00443-17>.
  38. Ingale, J., Stano, A., Guenaga, J., Sharma, S.K., Nemazee, D., Zwick, M.B., and Wyatt, R.T. (2016). High-Density Array of Well-Ordered HIV-1 Spikes on Synthetic Liposomal Nanoparticles Efficiently Activate B Cells. *Cell Rep.* 15, 1986–1999. <https://doi.org/10.1016/j.celrep.2016.04.078>.
  39. Zhang, P., Narayanan, E., Liu, Q., Tsybovsky, Y., Boswell, K., Ding, S., Hu, Z., Follmann, D., Lin, Y., Miao, H., et al. (2021). A multiclade env-gag VLP mRNA vaccine elicits tier-2 HIV-1-neutralizing antibodies and reduces the risk of heterologous SHIV infection in macaques. *Nat. Med.* 27, 2234–2245. <https://doi.org/10.1038/s41591-021-01574-5>.
  40. Dubrovskaya, V., Tran, K., Ozorowski, G., Guenaga, J., Wilson, R., Bale, S., Cottrell, C.A., Turner, H.L., Seabright, G., O'Dell, S., et al. (2019). Vaccination with Glycan-Modified HIV NFL Envelope Trimer-Liposomes Elicits Broadly Neutralizing Antibodies to Multiple Sites of Vulnerability. *Immunity* 51, 915–929.e7. <https://doi.org/10.1016/j.immuni.2019.10.008>.
  41. Cottrell, C.A., van Schooten, J., Bowman, C.A., Yuan, M., Oyen, D., Shin, M., Morpurgo, R., van der Woude, P., van Breemen, M., Torres, J.L., et al. (2020). Mapping the immunogenic landscape of near-native HIV-1 envelope trimers in non-human primates. *PLoS Pathog* 16, e1008753. <https://doi.org/10.1371/journal.ppat.1008753>.
  42. Huang, J., Kang, B.H., Pancera, M., Lee, J.H., Tong, T., Feng, Y., Imamiuchi, H., Georgiev, I.S., Chuang, G.Y., Druz, A., et al. (2014). Broad and potent HIV-1 neutralization by a human antibody that binds the gp41-gp120 interface. *Nature* 515, 138–142. <https://doi.org/10.1038/nature13601>.
  43. Scheid, J.F., Mouquet, H., Ueberheide, B., Diskin, R., Klein, F., Oliveira, T.Y., Pietzsch, J., Fenyo, D., Abadir, A., Velinzon, K., et al. (2011). Sequence and structural convergence of broad and potent HIV antibodies that mimic CD4 binding. *Science* 333, 1633–1637. <https://doi.org/10.1126/science.1207227>.
  44. Cingoz, O. (2009). Motavizumab. *MAbs* 1, 439–442. <https://doi.org/10.4161/mabs.1.5.9496>.
  45. Sok, D., van Gils, M.J., Pauthner, M., Julien, J.P., Saye-Francisco, K.L., Hsueh, J., Briney, B., Lee, J.H., Le, K.M., Lee, P.S., et al. (2014). Recombinant HIV envelope trimer selects for quaternary-dependent antibodies targeting the trimer apex. *Proc. Natl. Acad. Sci. USA* 111, 17624–17629. <https://doi.org/10.1073/pnas.1415789111>.
  46. Wu, X., Yang, Z.Y., Li, Y., Hogerkerp, C.M., Schief, W.R., Seaman, M.S., Zhou, T., Schmidt, S.D., Wu, L., Xu, L., et al. (2010). Rational design of envelope identifies broadly neutralizing human monoclonal antibodies to HIV-1. *Science* 329, 856–861. <https://doi.org/10.1126/science.1187659>.
  47. Seaman, M.S., Janes, H., Hawkins, N., Grandpre, L.E., Devoy, C., Giri, A., Coffey, R.T., Harris, L., Wood, B., Daniels, M.G., et al. (2010). Tiered categorization of a diverse panel of HIV-1 Env pseudoviruses for assessment of neutralizing antibodies. *J. Virol.* 84, 1439–1452. <https://doi.org/10.1128/JVI.02108-09>.
  48. Suloway, C., Pulokas, J., Fellmann, D., Cheng, A., Guerra, F., Quispe, J., Stagg, S., Potter, C.S., and Carragher, B. (2005). Automated molecular microscopy: the new Legimon system. *J. Struct. Biol.* 151, 41–60. <https://doi.org/10.1016/j.jsb.2005.03.010>.
  49. Emsley, P., and Cowtan, K. (2004). Coot: model-building tools for molecular graphics. *Acta Crystallogr D Biol Crystallogr* 60, 2126–2132. <https://doi.org/10.1107/S0907444904019158>.
  50. Zheng, S.Q., Palovcak, E., Armache, J.P., Verba, K.A., Cheng, Y., and Agard, D.A. (2017). MotionCorr2: anisotropic correction of beam-induced motion for improved cryo-electron microscopy. *Nat. Methods* 14, 331–332. <https://doi.org/10.1038/nmeth.4193>.
  51. Pettersen, E.F., Goddard, T.D., Huang, C.C., Couch, G.S., Greenblatt, D.M., Meng, E.C., and Ferrin, T.E. (2004). UCSF Chimera—a visualization system for exploratory research and analysis. *J. Comput. Chem.* 25, 1605–1612. <https://doi.org/10.1002/jcc.20084>.



52. Casañal, A., Lohkamp, B., and Emsley, P. (2020). Current developments in Coot for macromolecular model building of Electron Cryo-microscopy and Crystallographic Data. *Protein Sci.* 29, 1069–1078. <https://doi.org/10.1002/pro.3791>.
53. Adams, P.D., Gopal, K., Grosse-Kunstleve, R.W., Hung, L.W., Ioerger, T.R., McCoy, A.J., Moriarty, N.W., Pai, R.K., Read, R.J., Romo, T.D., et al. (2004). Recent developments in the PHENIX software for automated crystallographic structure determination. *J. Synchrotron Radiat.* 11, 53–55. [S0909049503024130 \[pii\]](https://doi.org/10.1107/S0909049503024130).
54. Lütteke, T., and von der Lieth, C.W. (2004). pdb-care (PDB carbohydrate residue check): a program to support annotation of complex carbohydrate structures in PDB files. *BMC Bioinf.* 5, 69. <https://doi.org/10.1186/1471-2105-5-69>.
55. Agirre, J., Iglesias-Fernández, J., Rovira, C., Davies, G.J., Wilson, K.S., and Cowtan, K.D. (2015). Privateer: software for the conformational validation of carbohydrate structures. *Nat. Struct. Mol. Biol.* 22, 833–834. <https://doi.org/10.1038/nsmb.3115>.
56. Barad, B.A., Echols, N., Wang, R.Y.R., Cheng, Y., DiMaio, F., Adams, P.D., and Fraser, J.S. (2015). EMRinger: side chain-directed model and map validation for 3D cryo-electron microscopy. *Nat. Methods* 12, 943–946. <https://doi.org/10.1038/nmeth.3541>.
57. Williams, C.J., Headd, J.J., Moriarty, N.W., Prisant, M.G., Videau, L.L., Deis, L.N., Verma, V., Keedy, D.A., Hintze, B.J., Chen, V.B., et al. (2018). MolProbity: More and better reference data for improved all-atom structure validation. *Protein Sci.* 27, 293–315. <https://doi.org/10.1002/pro.3330>.
58. Krissinel, E., and Henrick, K. (2007). Inference of macromolecular assemblies from crystalline state. *J. Mol. Biol.* 372, 774–797. <https://doi.org/10.1016/j.jmb.2007.05.022>.
59. Rawi, R., Rutten, L., Lai, Y.T., Olia, A.S., Blokland, S., Juraszek, J., Shen, C.H., Tsybovsky, Y., Verardi, R., Yang, Y., et al. (2020). Automated Design by Structure-Based Stabilization and Consensus Repair to Achieve Prefusion-Closed Envelope Trimers in a Wide Variety of HIV Strains. *Cell Rep.* 33, 108432. <https://doi.org/10.1016/j.celrep.2020.108432>.
60. Zhou, T., Teng, I.T., Olia, A.S., Cerutti, G., Gorman, J., Nazzari, A., Shi, W., Tsybovsky, Y., Wang, L., Wang, S., et al. (2020). Structure-Based Design with Tag-Based Purification and In-Process Biotinylation Enable Streamlined Development of SARS-CoV-2 Spike Molecular Probes. *Cell Rep.* 33, 108322. <https://doi.org/10.1016/j.celrep.2020.108322>.
61. Cottrell, C.A., Manne, K., Kong, R., Wang, S., Zhou, T., Chuang, G.Y., Edwards, R.J., Henderson, R., Janowska, K., Kopp, M., et al. (2021). Structural basis of glycan276-dependent recognition by HIV-1 broadly neutralizing antibodies. *Cell Rep.* 37, 109922. <https://doi.org/10.1016/j.celrep.2021.109922>.
62. Kwon, Y.D., Chuang, G.Y., Zhang, B., Bailer, R.T., Doria-Rose, N.A., Gindin, T.S., Lin, B., Louder, M.K., McKee, K., O'Dell, S., et al. (2018). Surface-Matrix Screening Identifies Semi-specific Interactions that Improve Potency of a Near Pan-reactive HIV-1-Neutralizing Antibody. *Cell Rep.* 22, 1798–1809. <https://doi.org/10.1016/j.celrep.2018.01.023>.
63. Mastrorade, D.N. (2005). Automated electron microscope tomography using robust prediction of specimen movements. *J. Struct. Biol.* 152, 36–51. <https://doi.org/10.1016/j.jsb.2005.07.007>.
64. Punjani, A., Rubinstein, J.L., Fleet, D.J., and Brubaker, M.A. (2017). cryo-SPARC: algorithms for rapid unsupervised cryo-EM structure determination. *Nat. Methods* 14, 290–296. <https://doi.org/10.1038/nmeth.4169>.
65. Jo, S., Kim, T., Iyer, V.G., and Im, W. (2008). CHARMM-GUI: a web-based graphical user interface for CHARMM. *J. Comput. Chem.* 29, 1859–1865. <https://doi.org/10.1002/jcc.20945>.
66. Jo, S., Song, K.C., Desaire, H., MacKerell, A.D., Jr., and Im, W. (2011). Glycan Reader: automated sugar identification and simulation preparation for carbohydrates and glycoproteins. *J. Comput. Chem.* 32, 3135–3141. <https://doi.org/10.1002/jcc.21886>.
67. Park, S.J., Lee, J., Patel, D.S., Ma, H., Lee, H.S., Jo, S., and Im, W. (2017). Glycan Reader is improved to recognize most sugar types and chemical modifications in the Protein Data Bank. *Bioinformatics* 33, 3051–3057. <https://doi.org/10.1093/bioinformatics/btx358>.
68. Park, S.J., Lee, J., Qi, Y., Kern, N.R., Lee, H.S., Jo, S., Jung, I., Joo, K., Lee, J., and Im, W. (2019). CHARMM-GUI Glycan Modeler for modeling and simulation of carbohydrates and glycoconjugates. *Glycobiology* 29, 320–331. <https://doi.org/10.1093/glycob/cwz003>.
69. Pettersen, E.F., Goddard, T.D., Huang, C.C., Meng, E.C., Couch, G.S., Croll, T.I., Morris, J.H., and Ferrin, T.E. (2021). UCSF ChimeraX: Structure visualization for researchers, educators, and developers. *Protein Sci.* 30, 70–82. <https://doi.org/10.1002/pro.3943>.
70. Ye, J., Ma, N., Madden, T.L., and Ostell, J.M. (2013). IgBLAST: an immunoglobulin variable domain sequence analysis tool. *Nucleic Acids Res.* 41, W34–W40. <https://doi.org/10.1093/nar/gkt382>.
71. Sethna, Z., Elhanati, Y., Callan, C.G., Walczak, A.M., and Mora, T. (2019). OLGA: fast computation of generation probabilities of B- and T-cell receptor amino acid sequences and motifs. *Bioinformatics* 35, 2974–2981. <https://doi.org/10.1093/bioinformatics/btz035>.
72. Soto, C., Bombardi, R.G., Branchizio, A., Kose, N., Matta, P., Sevy, A.M., Sinkovits, R.S., Gilchuk, P., Finn, J.A., and Crowe, J.E. (2019). High frequency of shared clonotypes in human B cell receptor repertoires. *Nature* 566, 398–402. <https://doi.org/10.1038/s41586-019-0934-8>.
73. Molé, C.M., Béne, M.C., Montagne, P.M., Seilles, E., and Faure, G.C. (1994). Light chains of immunoglobulins in human secretions. *Clin. Chim. Acta* 224, 191–197. [https://doi.org/10.1016/0009-8981\(94\)90185-6](https://doi.org/10.1016/0009-8981(94)90185-6).



## STAR★METHODS

### KEY RESOURCES TABLE

REAGENT or RESOURCE	SOURCE	IDENTIFIER
<b>Antibodies</b>		
0PV-c.01	Kong et al. <sup>17</sup>	N/A
N751-1B06	This study	N/A
N751-1C05	This study	N/A
N751-1C07	This study	N/A
1E6	Cottrell et al. <sup>41</sup>	N/A
N751-1F10	This study	N/A
N751-2B06	This study	N/A
N751-2C06	This study	N/A
N751-2C09	This study	N/A
N751-2D02	This study	N/A
35O22	Huang et al. <sup>42</sup>	N/A
3BNC117	Scheid et al. <sup>43</sup>	RRID: AB_2491033
5H3	Cottrell et al. <sup>41</sup>	N/A
A12V163-a.01	Kong et al. <sup>17</sup>	N/A
A12V163-b.01	Kong et al. <sup>17</sup>	N/A
Motavizumab	Cingoz <sup>44</sup>	RRID: AB_2910856
PGDM1400	Sok et al. <sup>45</sup>	N/A
PGT122	Walker et al. <sup>10</sup>	RRID: AB_2491042
PGT151	Blattner et al. <sup>31</sup>	N/A
vFP16.02	Xu et al. <sup>30</sup>	N/A
VRC01	Wu et al. <sup>46</sup>	RRID: AB_2491019
VRC34.01	Kong et al. <sup>8</sup>	RRID: AB_2819225
<b>Chemicals, peptides, and recombinant proteins</b>		
Pierce Protein A Agarose	ThermoFisher Scientific	20334
Turbo293 transfection reagent	SPEED BioSystem	PXX1002
AbBooster medium	ABI scientific	PB2668
<b>Bacterial and virus strains</b>		
BG505	NIH/VRC	N/A
BG505.N611Q	NIH/VRC	N/A
BG505.S241N	NIH/VRC	N/A
<b>Deposited data</b>		
2C06-BG505 DS-SOSIP structure	This study	PDB: 8G4M
2C06-BG505 DS-SOSIP maps	This study	EMDB: EMD-29725
2C09-BG505 DS-SOSIP structure	This study	PDB: 8G4T
2C09-BG505 DS-SOSIP maps	This study	EMDB: EMD-29731
<b>Experimental models: Cell lines</b>		
293F Freestyle cells	Thermo Fisher	K900001
Expi293F cells	Thermo Fisher	A14527
<b>Recombinant DNA</b>		
pVRC8400-1B06 plasmids	This study	N/A
pVRC8400-1C05 plasmids	This study	N/A
pVRC8400-1C07 plasmids	This study	N/A
pVRC8400-1C07 plasmids	This study	N/A

(Continued on next page)

**Continued**

REAGENT or RESOURCE	SOURCE	IDENTIFIER
pVRC8400-1F10 plasmids	This study	N/A
pVRC8400-2B06 plasmids	This study	N/A
pVRC8400-2C06 plasmids	This study	N/A
pVRC8400-2C09 plasmids	This study	N/A
pVRC8400-2D02 plasmids	This study	N/A

**Software and algorithms**

Chimera	Pettersen et al. <sup>47</sup>	<a href="https://www.cgl.ucsf.edu/chimera/">https://www.cgl.ucsf.edu/chimera/</a>
ChimeraX	Pettersen et al. <sup>48</sup>	<a href="https://www.cgl.ucsf.edu/chimerax/">https://www.cgl.ucsf.edu/chimerax/</a>
Coot	Emsley and Cowtan <sup>49</sup>	<a href="https://sbgrid.org/software/">https://sbgrid.org/software/</a>
CryoSparc	Punjani et al. <sup>50</sup>	<a href="https://guide.cryosparc.com/">https://guide.cryosparc.com/</a>
IgBlast	Ye et al. <sup>51</sup>	<a href="https://www.ncbi.nlm.nih.gov/igblast/">https://www.ncbi.nlm.nih.gov/igblast/</a>
Leginon software	Suloway et al. <sup>52</sup>	<a href="https://emg.nysbc.org/redmine/projects/leginon/wiki/Leginon_Homepage">https://emg.nysbc.org/redmine/projects/leginon/wiki/Leginon_Homepage</a>
MolProbity	Barad et al.; Williams et al. <sup>53,54</sup>	<a href="http://molprobity.biochem.duke.edu">http://molprobity.biochem.duke.edu</a>
OLGA	Sethna et al. <sup>55</sup>	<a href="https://github.com/statbiophys/OLGA">https://github.com/statbiophys/OLGA</a>
PDBePISA	Krissinel et al. <sup>56</sup>	<a href="https://www.ebi.ac.uk/pdbe/pisa/">https://www.ebi.ac.uk/pdbe/pisa/</a>
Phenix	Adams et al. <sup>57</sup>	<a href="https://sbgrid.org/software/">https://sbgrid.org/software/</a>
PRISM	GraphPad Software	<a href="https://www.graphpad.com/scientific-software/prism/">https://www.graphpad.com/scientific-software/prism/</a>
Pymol	Schrödinger LLC	<a href="https://pymol.org">https://pymol.org</a>
SerialEM 4.0	Mastronarde <sup>58</sup>	<a href="https://bio3d.colorado.edu/SerialEM/">https://bio3d.colorado.edu/SerialEM/</a>

**RESOURCE AVAILABILITY**

**Lead contact**

Further information and requests for resources and reagents should be directed to and will be fulfilled by Peter D. Kwong ([pdkwong@nih.gov](mailto:pdkwong@nih.gov)).

**Materials availability**

Plasmids generated in this study are available upon request.

**Data and code availability**

- Cryo-EM maps have been deposited to the EMDB with accession codes EMD-29725 and EMD-29731, and fitted coordinates have been deposited to PDB with accession codes 8G4M and 8G4T.
- This paper does not report original code.
- Any additional information required to reanalyze the data reported in this paper is available from the [lead contact](#) upon request.

**EXPERIMENTAL MODEL AND SUBJECT DETAILS**

**Serum samples**

The samples were collected under the Vaccine Research Center's (VRC), National Institute of Allergy and Infectious Diseases (NIAID), National Institutes of Health protocol VRC 018 (NCT03783130) in compliance with the NIH Institutional Review Board (IRB) approved protocol and procedures. All subjects met protocol eligibility criteria and agreed to participate in the study by signing the NIH IRB approved informed consent. Research studies with these samples were conducted by protecting the rights and privacy of the study participants.

**Cell lines**

HEK293F, Expi293F and FreeStyle 293-F cells were purchased from Thermo Fisher Scientific. The cells were used directly from the commercial sources following manufacturer suggestions as described in detail below.

## METHOD DETAILS

### Preparation of Env trimers and antigen-specific probes

BG505 DS-SOSIP and ConC trimers were expressed in stable CHO cell lines and purified by non-affinity chromatography.<sup>21</sup> Glycan-base BG505 was stabilized in prefusion-closed conformation by structure-based stabilization and consensus repair.<sup>59</sup> Biotinylated probes of BG505 DS-SOSIP, glycan-base BG505, ConC, and glycan-base BG505-N241 were expressed in 293Freestyle cells as a fusion protein with an N-terminal single-chain Fc tag cleavable by HRV3C digestion and an AVI-tag at C terminus.<sup>60</sup> Cell supernatants were harvested, and the proteins were bound on a protein A column, washed, N-terminal Fc tag cleaved, biotinylated, and eluted. The eluted proteins were passed through a Superdex 200 16/600 column with PBS, and the biotinylated proteins were conjugated to fluorescent streptavidin.

### B cell sorting

Cryopreserved PBMC from VRC 018 clinical trial ([ClinicalTrials.gov](https://clinicaltrials.gov/ct2/show/study/NCT03783130) NCT03783130)<sup>22</sup> at 2 weeks after third boost time point were thawed, treated with Benzonase nuclease (Millipore Corp.), washed with PBS and stained with viability dye Aqua Fluorescent Reactive (Invitrogen) for 2 min followed by staining with the following human antibodies: anti-IgM-BB700 (BD, customized), anti-CD21-PE594 (BD Biosciences, 563474), anti-CD20-APCH7 (BD Biosciences, 560734), anti-IgG-BUV3950 (BD Biosciences, 564229), anti-CD3-BV510 (BD Biosciences, 740187), anti-CD14-BV510 (Biolegend, 301842), anti-CD56-BV510 (BD Biosciences, 740171), anti-CD38-BUV661 (BD Biosciences, 612969), anti-CD19-BUV805 (BD Biosciences, 749173), anti-IgD-BV570 (BD Biosciences, 624298), anti-CD27-BV605 (Biolegend, 302830) along with BG505-AF488, glycan-base BG505-PE and glycan-base BG505-APC probes diluted in Brilliant Stain Buffer (BD Biosciences, 563794) for 30 min at 4°C protected from light. Cells were washed with PBS containing 0.1% BSA twice and analyzed on FACS Symphony A5 (BD Biosciences) using Diva software. Cells were gated on live singlets CD3<sup>+</sup> CD4<sup>+</sup> CD14<sup>+</sup> CD56<sup>+</sup> IgD<sup>-</sup> IgM<sup>-</sup> CD19<sup>+</sup> CD20<sup>+</sup> IgG<sup>+</sup> memory B cells and all glycan-base BG505 positive cells were single-cell sorted in 96-well plates coated with 5 μL of TCL buffer (Qiagen) containing 1% of 2-Mercaptoethanol (Sigma-Aldrich).

### Rapid assembly, transfection, and production of immunoglobulins (RATP-Ig)

The sorted B cells were subjected to RATP-Ig following the procedures as described previously.<sup>25</sup> Briefly, single-cell RNA was purified with RNAClean beads (Beckman Coulter). cDNA was then synthesized using 5' RACE reverse-transcription and amplified by PCR, and heavy and light chain variable regions enriched. An aliquot of enriched cDNA was sequenced using 2 × 150 paired-end reads on an Illumina MiSeq. For immunoglobulin production, enriched variable regions were assembled into expression cassettes that include CMV, and HC/LC-TBGH polyA fragments. Assembled cassettes were amplified by PCR and transfected into Expi293 cells in 96-well deep-well plates using the Expi293 Transfection Kit (ThermoFisher Scientific). Cell cultures were grown at 37°C, 8% CO<sub>2</sub>, and 1100 RPM shaking for 5–7 days. Cell culture supernatants were harvested by centrifugation.

### AlphaLISA screening of RATP-Ig supernatants

RATP-Ig supernatants from glycan-base BG505-positive B cells were diluted into AlphaLISA buffer (PBS + 0.05% Tween 20 + 0.5 mg/mL BSA), and 5 μL of each were transferred to an OptiPlate-384 assay plate (white opaque, PerkinElmer, Waltham, MA). To each well was added 10 μL of biotinylated Env trimer probe at 10 nM final concentration and 10 μL of anti-human Fc IgG (PerkinElmer, Waltham, MA) acceptor beads at 10 μg/mL final concentration. The mixtures were incubated at room temperature (RT) for an hour and then added 25 μL of streptavidin donor beads (PerkinElmer, Waltham, MA) at 40 μg/mL final concentration. The plate was incubated at RT for 30 min in the dark, and the AlphaLISA signal was read using a SpectraMax i3x multi-mode microplate reader (Molecular Devices, San Jose, CA). Only nine supernatants out of two plates of RATP-Ig supernatants were identified as double-positive for binding BG505 DS-SOSIP and glycan-base BG505, likely due to both false positives in B cell sorting and low level of Ig expression in RATP-Ig for some antibodies.

### Antibody preparation

DNA encoding antibody heavy- and light-chain variable regions were synthesized and cloned into the pVRC8400 vectors.<sup>61</sup> Plasmids of heavy and light chain pairs were co-transfected in Expi293F cells (Thermo Fisher) using Turbo293 transfection reagent (Speed BioSystems) as described previously.<sup>62</sup> On day 6 post transfection, the culture supernatant was harvested and loaded on a protein A column. The column was washed with PBS, and the IgG protein was eluted with a low pH buffer. For Fab preparation, an HRV3C cleavage site was inserted in the heavy-chain hinge region in the pVRC8400 vectors. The eluted IgG protein was digested with HRV3C, and the Fab was purified from a protein A column and then further purified from a Superdex 200 column (Cytiva).

### Env-pseudovirus neutralization assays

Monoclonal antibody neutralization was assessed based on the single-round infection assay of TZM-bl cells with HIV-1 Env-pseudoviruses as described previously.<sup>47</sup> Purified monoclonal antibodies were tested for neutralization against wild-type HIV-1 strains and the glycan mutants of BG505. Data were calculated as half-maximum inhibitory concentration (IC<sub>50</sub>) and 80% maximum inhibitory concentration (IC<sub>80</sub>) by comparison with control wells in the absence of antibodies.

### Enzyme-linked immunosorbent assay (ELISA)

Anti-fusion peptide ELISA was performed by coating 96-well plates (Costar High Binding Half-Area; Corning, Kennebunk, ME) overnight at 4°C with 50  $\mu$ L/well of 2  $\mu$ g/mL FP8v1-rTTHC (AVGIGAVF), FP7v1-rTTHC (AVGIGAV), or FP6v1-rTTHC (AVGIGA) in PBS. Between each subsequent step, plates were washed five times with PBS-T (PBS plus 0.05% Tween) unless otherwise stated. Plates were blocked with 100  $\mu$ L/well of in-house B3T blocking solution (30 mM NaCl, 10 mM Tris-HCl, 0.2 mM EDTA, 0.66% fetal bovine serum [FBS], 0.4% bovine albumin, 0.014% Tween 20, 0.004% thimerosal) for 1 h at 37°C. Next, 50  $\mu$ L/well of serially diluted 2C06 or 2C09 antibody (7-point, 5-fold, 2  $\mu$ g/mL starting concentration) were added to the plates and incubated for 1 h at 37°C. Goat anti-human IgG  $\gamma$ -chain horseradish peroxidase conjugated secondary antibody (Jackson ImmunoResearch, West Grove, PA) diluted 1:5000 in B3T blocking solution was added to the plates (50  $\mu$ L/well) and incubated for 1 h at 37°C. Next, plates were developed with 50  $\mu$ L/well tetramethylbenzidine (TMB) substrate (SureBlue; KPL, Gaithersburg, MD) for 10 min at RT, and the reaction was stopped with 50  $\mu$ L/well 1 N sulfuric acid (Fisher Chemical, Fair Lawn, NJ) without washing. Plates were read at 450 nm (SpectraMax using SoftMax Pro, Version 5, software; Molecular Devices, Sunnyvale, CA), and the optical densities (OD) were analyzed following subtraction of the non-specific horseradish peroxidase background activity.

Competition ELISA for antibody binding to BG505 DS-SOSIP was performed by coating 96-well plates (Costar High Binding Half-Area; Corning, Kennebunk, ME) overnight at 4°C with 50  $\mu$ L/well of 2  $\mu$ g/mL snowdrop lectin from *Galanthus nivalis* (Sigma-Aldrich, St. Louis, MO) in PBS. Between each subsequent step, plates were washed five times with PBS-T (PBS plus 0.05% Tween) unless otherwise stated. Following lectin coating, plates were blocked with 100  $\mu$ L/well of blocking buffer (5% skim milk in PBS) (Fisher Scientific, Waltham, MA) for 1 h at RT. Blocking was followed by trimer capture with 50  $\mu$ L/well of 2  $\mu$ g/mL BG505 DS-SOSIP in FBS-PBS diluent (PBS plus 10% FBS) for 2 h at RT. Next, 50  $\mu$ L/well mouse Fc competitor antibodies targeting several important trimer epitopes (fusion peptide, V1V2 region, CD4 binding site, V3 glycan, gp120/gp41 interface, or trimer base) were added at a fixed concentration of 2  $\mu$ g/mL in blocking buffer and incubated for 1 h at RT. Without washing the plate, 50  $\mu$ L/well of serially diluted 2C06 or 2C09 antibody (7-point, 5-fold, 2  $\mu$ g/mL starting concentration) were added to the plates and incubated for 1 h at RT. Next, goat anti-human IgG  $\gamma$ -chain horseradish peroxidase conjugated secondary antibody (Jackson ImmunoResearch, West Grove, PA) diluted 1:5000 in blocking buffer was added to the plates (50  $\mu$ L/well) and incubated for 1 h at RT. Next, plates were developed with 50  $\mu$ L/well TMB substrate (SureBlue; KPL, Gaithersburg, MD) for 10 min at RT, and the reaction was stopped with 50  $\mu$ L/well 1 N sulfuric acid (Fisher Chemical, Fair Lawn, NJ) without washing. Plates were read at 450 nm (SpectraMax using SoftMax Pro, Version 5, software; Molecular Devices, Sunnyvale, CA), and the optical densities (OD) were analyzed following subtraction of the non-specific horseradish peroxidase background activity. Area under the curve (AUC) values of 2C06 or 2C09 were calculated from reciprocal dilution curves in the competition assay (GraphPad Prism 9.4.1 software). AUC values of 2C06 or 2C09 binding in the absence of competitor antibody represent unblocked trimer binding from which AUC values of 2C06 or 2C09 binding in the presence of competitor antibody were subtracted. This value was divided by unblocked trimer binding AUC and multiplied by 100 to obtain the percent reduction in trimer binding. Measurements were carried out in triplicates; mean and SE are reported.

### IgG binding affinity measured by Carterra

A medium density HC30M sensor chip was preconditioned with 1-min pulses of each of three solutions: 50 mM NaOH, 1 M NaCl, and 10 mM Glycine pH 2.0. After preconditioning, the chip was activated with a 10-min injection of a freshly prepared 1:1:1 (v/v/v) mixture of 0.4 M 1-ethyl-3-(3-dimethylaminopropyl) carbodiimide hydrochloride (EDC), 0.1 M *N*-hydroxysulfosuccinimide (sNHS) and 0.1 M 2-(*N*-morpholino) ethanesulfonic acid (MES) pH 5.5. Then, 100  $\mu$ g/mL of goat anti-human Fc antibody prepared in 10 mM sodium acetate pH 4.5 + 0.01% Tween 20 was coupled for 15 min and the excess reactive esters were blocked with 1 M ethanolamine HCl pH 8.5 during a 5 min injection. Antibodies were prepared at 10  $\mu$ g/mL in running buffer (10 mM HEPES pH 7.4, 150 mM NaCl, 3 mM EDTA, and 0.01% (v/v) Tween 20 (HBSTE) supplemented with 0.5 mg/mL BSA) and captured for 15 min. The antigens (BG505 DS-SOSIP and glycan-base BG505) were then prepared at 0, 3.9, 7.8, 15.6, 31.2, 62.5, 125, 250, and 500 nM in HBSTE +0.5 mg/mL BSA and injected with an association time of 5 min, followed by a 15 min dissociation. Samples were injected in ascending concentration and the surface was regenerated with IgG elution buffer (glycine, pH 2.8) after finishing the concentration series of each antigen. Binding data from the local reference spots was used to subtract signal from the active spots and the nearest buffer blank analyte responses were subtracted to double-reference the data. The double-referenced data were fitted to a simple 1:1 Langmuir binding model in Carterra's Kinetic Inspection Tool.

### Bio-layer interferometry (BLI)

An Octet RED instrument (FortéBio) instrument was used to measure recognition of isolated antibodies to HIV-1 BG505 DS-SOSIP, glycan-base BG505, ConC and glycan-base BG505-N241 trimers. Isolated antibodies (50  $\mu$ g/mL) were immobilized for 300 s on AHC biosensor tips and equilibrated for 60 s in Octet Kinetics Buffer (Sartorius Corporation) prior to measuring association with HIV-1 trimer diluted in Octet Kinetics Buffer (100  $\mu$ g/mL). The association of HIV-1 trimers were recorded for 300 s. All BLI experiments were conducted at 30°C and were performed in duplicate. Parallel correction to subtract systematic baseline drift was carried out by subtracting the measurements recorded for a loaded sensor incubated in Octet Kinetics Buffer. Response levels of sensors were analyzed using Octet and GraphPad Prism 9 software.



### Surface plasmon resonance measurements of Fab binding affinity

Binding affinities and kinetics of 2C06 and 2C09 antibodies were assessed by surface plasmon resonance (SPR) on a Biacore S-200 (GE Healthcare) at 25°C in HBS-P+ buffer (10 mM HEPES, pH 7.4, 150 mM NaCl and 0.05% surfactant P-20). Glycan-reactive 2G12 IgG was immobilized onto a CM5 chip by amine coupling to 8000–10000 response units (RU). BG505 DS-SOSIP at 25 nM were captured to the sample channel at 300 RU on the 2G12 sensor chip. Serial two-fold diluted 2C06 and 2C09 Fabs were passed through the sample and reference channels for 180 s followed by a 300 s dissociation phase at 30  $\mu$ L/min. The surface was regenerated by flowing 3 M MgCl<sub>2</sub> solution for 30 s at a flow rate of 50  $\mu$ L/min. Blank sensorgrams were obtained by injection of the same volume of HBS-P+ buffer in place of antibody Fab solution. Sensorgrams of the concentration series were corrected with corresponding blank curves.

### Cryo-EM sample preparation and data collection

Samples for cryo-EM grid preparation of the 2C06-BG505 DS-SOSIP complex were produced by first mixing 15  $\mu$ L of purified BG505 SOSIP at 4 mg/mL with 55  $\mu$ L of 2C06 Fab at 1 mg/mL; n-Dodecyl  $\beta$ -D-maltoside (DDM) was added to have a final concentration of 0.005% (w/v) to prevent preferred orientation and aggregation during vitrification, and the mixture was incubated on ice for 20 min. Cryo-EM grids were prepared by applying 3  $\mu$ L of sample to a freshly glow discharged carbon-coated copper grid (CF 1.2/1.3 300 mesh). The sample was vitrified in liquid ethane using a Vitrobot Mark IV with a wait time of 30 s, a blot time of 3 s, and a blot force of 0. Cryo-EM data were collected using Leginon software<sup>48</sup> on a Titan Krios electron microscope operating at 300 kV, equipped with a Gatan K3-BioQuantum direct detection device. Exposures were taken with a total electron fluence of 58.06 e<sup>-</sup>/Å<sup>2</sup>. The total dose was fractionated for 2.5 s over 50 raw frames.

For preparing the 2C09-BG505 DS-SOSIP complexes, Env was mixed with the antibody Fab at 1 to 1.2 M ratio at a final total protein concentration of  $\sim$ 3 mg/mL; DDM (1 mM stock solution) was added to a final concentration of 0.1 mM. 2.7  $\mu$ L of the mixture was pipetted to a Quantifoil-gold 2/2 holey carbon grids, glow discharged for 30 s in a PELCO easiGlow Glow Discharge Cleaning System prior to cryo-grid preparation, and the grid was blotted for 2.5–4 s and plunge frozen into liquid ethane using a Vitrobot Mark IV (ThermoFisher). Cryo-EM data were collected on a Titan Krios operating at 300 kV, equipped with a K2 Summit detector (Gatan) operating in counting mode. Data were acquired using SerialEM 4.0.<sup>63</sup> The dose was fractionated over 40 raw frames.

The movie frames were aligned and dose-weighted<sup>50</sup> using cryoSPARC 3.3,<sup>64</sup> and CTF estimation, particle picking, 2D classifications, *ab initio* model generation, heterogeneous refinements, homogeneous 3D refinements, non-uniform refinement, and local resolution calculations were carried out using cryoSPARC 3.3.

### Model building and refinement

For structural determination, a model of the antibody Fab was generated using AlphaFold2 python notebook ([https://colab.research.google.com/github/sokrypton/ColabFold/blob/main/beta/AlphaFold2\\_advanced.ipynb](https://colab.research.google.com/github/sokrypton/ColabFold/blob/main/beta/AlphaFold2_advanced.ipynb)). The Fab model and the structure of BG505 DS-SOSIP (PDB: 6cdi)<sup>30</sup> were docked into the cryo-EM density map using UCSF Chimera<sup>51</sup> to build an initial model of the complex. The model was then manually rebuilt to the best fit into the density using Coot<sup>52</sup> and refined using Phenix.<sup>53</sup> Glycan structures were validated using Privateer and pdb-care.<sup>54,55</sup> Alternative glycan conformations were modeled by Glycan Reader & Modeler of CHARMM-GUI.<sup>65–68</sup> Overall structures were evaluated using MolProbity.<sup>56,57</sup> Protein interface calculations were performed using PISA.<sup>58</sup> Structural figures were generated using PyMOL (Schrödinger; <http://www.pymol.org>) and UCSF ChimeraX.<sup>69</sup>

### Antibody recombination and sequence signature analyses

IgBlast was used to annotate antibody germline gene and to analyze V(D)J recombination event.<sup>70</sup> The buried surface area (BSA) at the antibody-Env interface was calculated with PDBePISA.<sup>58</sup> The structure-based process used to identify sequence signature for classifying antibodies was as previously described.<sup>29</sup> Briefly, for antibodies with similar binding mode, we defined sequence motif by residues with a BSA value larger than 10 Å<sup>2</sup>. We compared sequence motifs that had similar recognition. Then, such sequence motifs with compatible VH/VL germline genes were selected as the sequence signature.

The precursor frequency was calculated using OLGA software.<sup>71</sup> Three healthy donor NGS samples were used to learn the model.<sup>72</sup> We used frequency of 60% for heavy chain pairing with kappa light chain (with a frequency of 40% for pairing with lambda light chains).<sup>73</sup>

### QUANTIFICATION AND STATISTICAL ANALYSIS

Cryo-EM data were processed and analyzed using CryoSparc. Cryo-EM structural statistics were analyzed with Phenix and Molprobity. Statistical details of experiments are described in [method details](#) or figure legends.

**Supplemental information**

**HIV-1 neutralizing antibodies elicited in humans  
by a prefusion-stabilized envelope trimer form  
a reproducible class targeting fusion peptide**

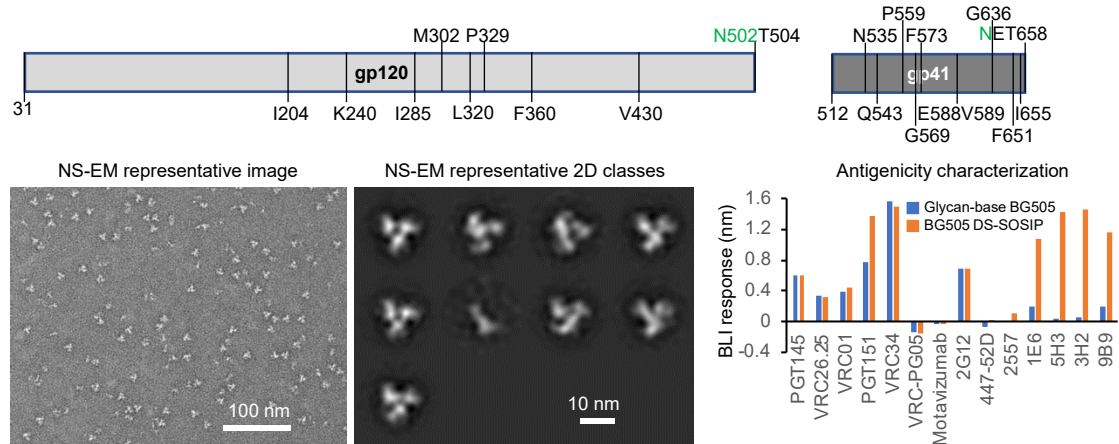
**Shuishu Wang, Flavio Matassoli, Baoshan Zhang, Tracy Liu, Chen-Hsiang Shen, Tatsiana Bylund, Timothy Johnston, Amy R. Henry, I-Ting Teng, Prabhanshu Tripathi, Jordan E. Becker, Anita Changela, Ridhi Chaudhary, Cheng Cheng, Martin Gaudinski, Jason Gorman, Darcy R. Harris, Myungjin Lee, Nicholas C. Morano, Laura Novik, Sijy O'Dell, Adam S. Olia, Danealle K. Parchment, Reda Rawi, Jesmine Roberts-Torres, Tyler Stephens, Yaroslav Tsybovsky, Danyi Wang, David J. Van Wazer, Tongqing Zhou, Nicole A. Doria-Rose, Richard A. Koup, Lawrence Shapiro, Daniel C. Douek, Adrian B. McDermott, and Peter D. Kwong**

### A Env trimers used for B cell sorting and antibody-binding analyses

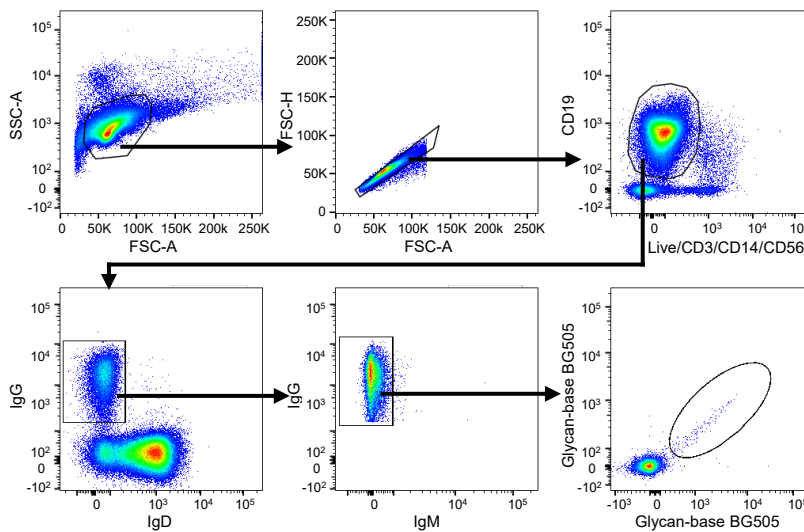


### B Glycan-base BG505 design and characterization

Glycan-base BG505 sequence - relative to BG505 DS-SOSIP, additional stabilizing mutations and two *N*-glycans at trimer base



### C Sorting gates



### D Staining of IgG+ cells

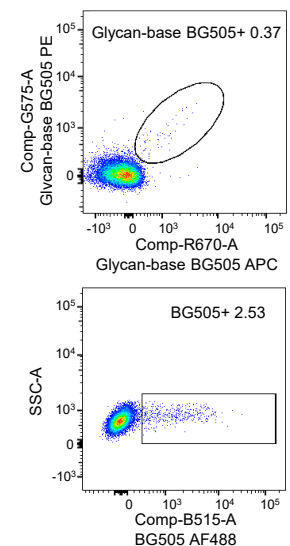


**Figure S1. Env trimers and B cell sorting details, related to Figure 1.**

(A) Env trimers used for B cell sorting and binding analyses with AlphaLISA, BLI, and SPR.

(B) The probe glycan-base BG505 was designed based on BG505 DS-SOSIP with additional mutations to stabilize the trimer in prefusion-closed conformation and two additional *N*-glycans to cover the trimer base. Negative stain (NS) EM revealed well-formed trimers, but with some monomeric shape present. Glycan-base BG505 bound most antibodies similarly to BG505 DS-SOSIP, except for the base-directed antibodies 1E6, 5H3, 3H2, and 9B9, to which it had negligible affinity.

(C) Details of B cell sorting gate strategy.

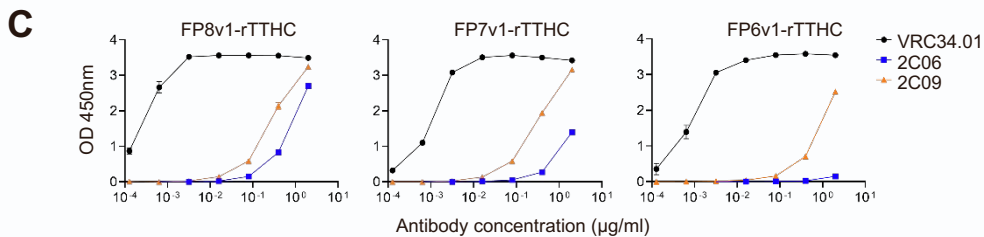
(D) Cytometry of IgG+ B cells from N751 serum. Cells were stained first with glycan-base BG505 to allow all non-base directed B cells to engage first in the trimer, washed the cells, and then stained with BG505 to allow the base-specific B cells to engage. BG505+ cell population is much larger than glycan-base BG505+ cell population. The glycan-base BG505-positive cells account for 0.37% of IgG+ memory B cells (Singlet, Live, CD19+, CD3-, CD14-, CD56-, IgG+) (upper panel). After absorption with glycan-base BG505, 2.53% of IgG+ memory B cells bind BG505 DS-SOSIP trimer (lower panel). Glycan-base BG505+ cells are 12.89% of all antigen-specific memory B cells, and the other 87.11% are likely targeting the trimer base.

### A Pseudovirus neutralization assessments for 2D02 and 1B06

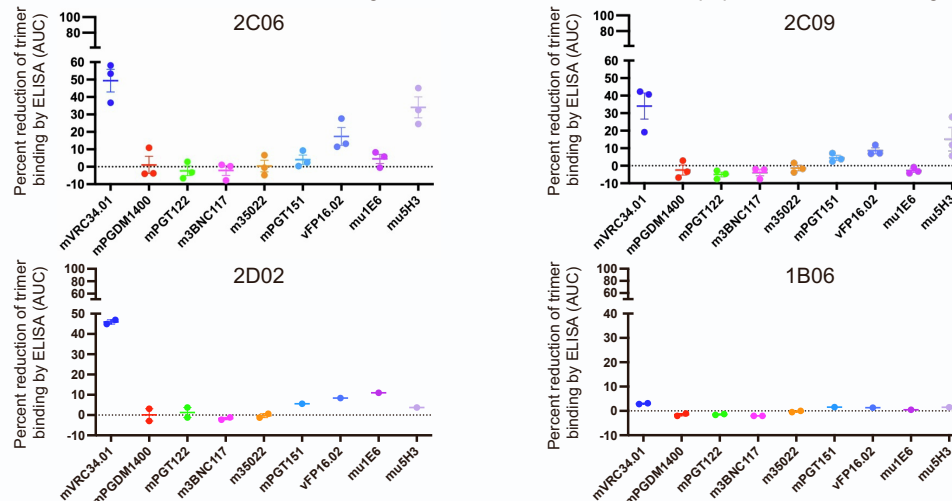
Viral strains	IC50 $\mu\text{g/ml}$			IC80 $\mu\text{g/ml}$		
	MW965.26	BG505.W6M.C2	BG505.W6M.C2.N611Q	MW965.26	BG505.W6M.C2	BG505.W6M.C2.N611Q
Clade	C	A		C	A	
2D02 IgG	>50	>50	>50	>50	>50	>50
1B06 IgG	>50	>50	>50	>50	>50	>50

### B Neutralization assessments against a panel of viruses neutralized by most fusion peptide-directed antibodies

Viral strains	Clade	BG505.W6M.C2.N611Q	BG505.W6M.C2	HxB2.D.G	KER200.8.12	MB201.A1	MI369.A5	96ZM6.51.02	CNE40	Q23.17	CH117.4	3468.V.1.C12	3365.v2.c20	2M135.10a	BI369.9A	0815.v.3.c3	CNE19
		A	A	B	A	A	A	C	BC	A	BC	AD	A	C	A	ACD	BC
IC50 $\mu\text{g/ml}$	2C06 IgG	2.92	33.6	>100	>100	>100	>100	>100	>100	>100	>100	>100	>100	>100	>100	>100	>100
	2C09 IgG	2.07	44.2	>100	>100	>100	>100	>100	>100	>100	>100	>100	>100	>100	>100	>100	>100
	N123-VRC34.01	0.017	0.116	0.254	0.082	0.072	0.155	0.121	0.214	0.173	0.062	1.11	0.050	>100	0.134	0.039	0.035
IC80 $\mu\text{g/ml}$	2C06 IgG	10.4	>100	>100	>100	>100	>100	>100	>100	>100	>100	>100	>100	>100	>100	>100	>100
	2C09 IgG	10.9	>100	>100	>100	>100	>100	>100	>100	>100	>100	>100	>100	>100	>100	>100	>100
	N123-VRC34.01	0.084	0.641	1.05	0.317	0.323	1.03	0.414	0.832	1.21	0.604	>100	0.194	>100	1.25	0.14	>100



### D Competition ELISA of 2C06 and 2C09 binding to BG505 DS-SOSIP with fusion peptide and base-binding antibodies



### E Neutralization assessments against BG505.S241N as well as against all strains in 208-strain panel lacking a glycan at residue 241

Viral strains	BG505.S241N	CNE56	929-28	T257-31	0077.v1.c16	3168.v4.c10	6471.v1.c16	25710-2.43
	Tier 2	2	2/3	2	C	C	C	1B/2
Clade	A	AE	AG	AG	C	C	C	C
IC50 $\mu\text{g/ml}$	2C06	>100	>100	>100	>100	>100	>100	>100
	2C09	>100	>100	>100	>100	>100	>100	>100
	VRC34.01	0.758	>100	>100	>100	1.48	11.5	>100
IC80 $\mu\text{g/ml}$	2C06	>100	>100	>100	>100	>100	>100	>100
	2C09	>100	>100	>100	>100	>100	>100	>100
	VRC34.01	4.610	>100	>100	>100	>100	65.6	>100

**Figure S2. Binding and neutralization data, related to Figures 1, 5, and 6.**

(A) Neutralization assessments for 2D02 and 1B06 revealed no detectable neutralization activity.

(B) Neutralization assessments of VRC 018-elicited antibodies from donor N751 against a panel of viruses neutralized by most fusion peptide-directed antibodies.

(C) ELISA analysis of 2C06 and 2C09 IgG binding to fusion peptide. Measurements were carried out in triplicates, and mean and SE are reported for each data point.

(D) Competition ELISA revealed 2C06, 2C09, and 2D02 competed for binding to BG505 DS-SOSIP trimer with fusion peptide-directed antibodies and base binding antibody 1E6 or 5H3, whereas 1B06 did not compete with any antibody tested.

(E) Neutralization assessments focusing on strains in 208-strain panel lacking a glycan at residue 241.



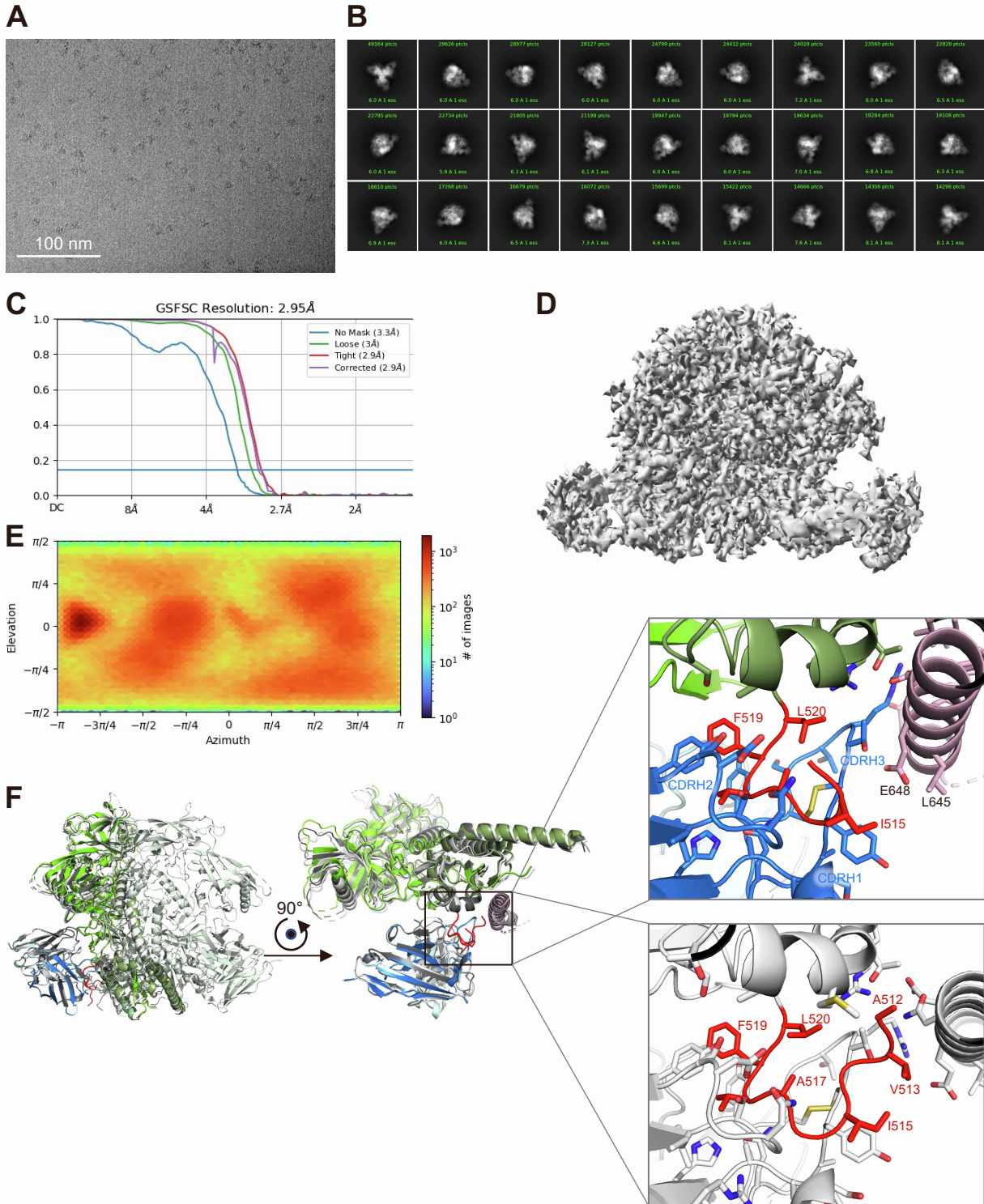


**Figure S3. Cryo-EM validation for 2C06 in complex with BG505 DS-SOSIP, related to Figure 2.**

(A) Representative micrograph. (B) 2D classes. (C) Fourier shell correlation (FSC) curves showing gold-standard FSC resolution at 2.95 Å. (D) 3D reconstruction density map at 2.95 Å from non-uniform refinement with C1 symmetry, showing antibody Fab binding near the trimer base at the fusion peptide-site of vulnerability. (E) Orientations of all particles used in the final refinement shown as a heatmap. (F) Superposition of three protomers revealing the trimer asymmetry induced by 2C06 binding. (Left) Protomers in right and back are superimposed on the one in left. (Middle) A 90° rotation of the left image to put the superimposed antibody chains at the bottom. Only the superimposed protomers are shown. One protomer is shown in colors, and the other two are in light or dark gray. (Right) Zoom-in views showing two slightly different modes of binding. The helix on the right is from a neighboring protomer.

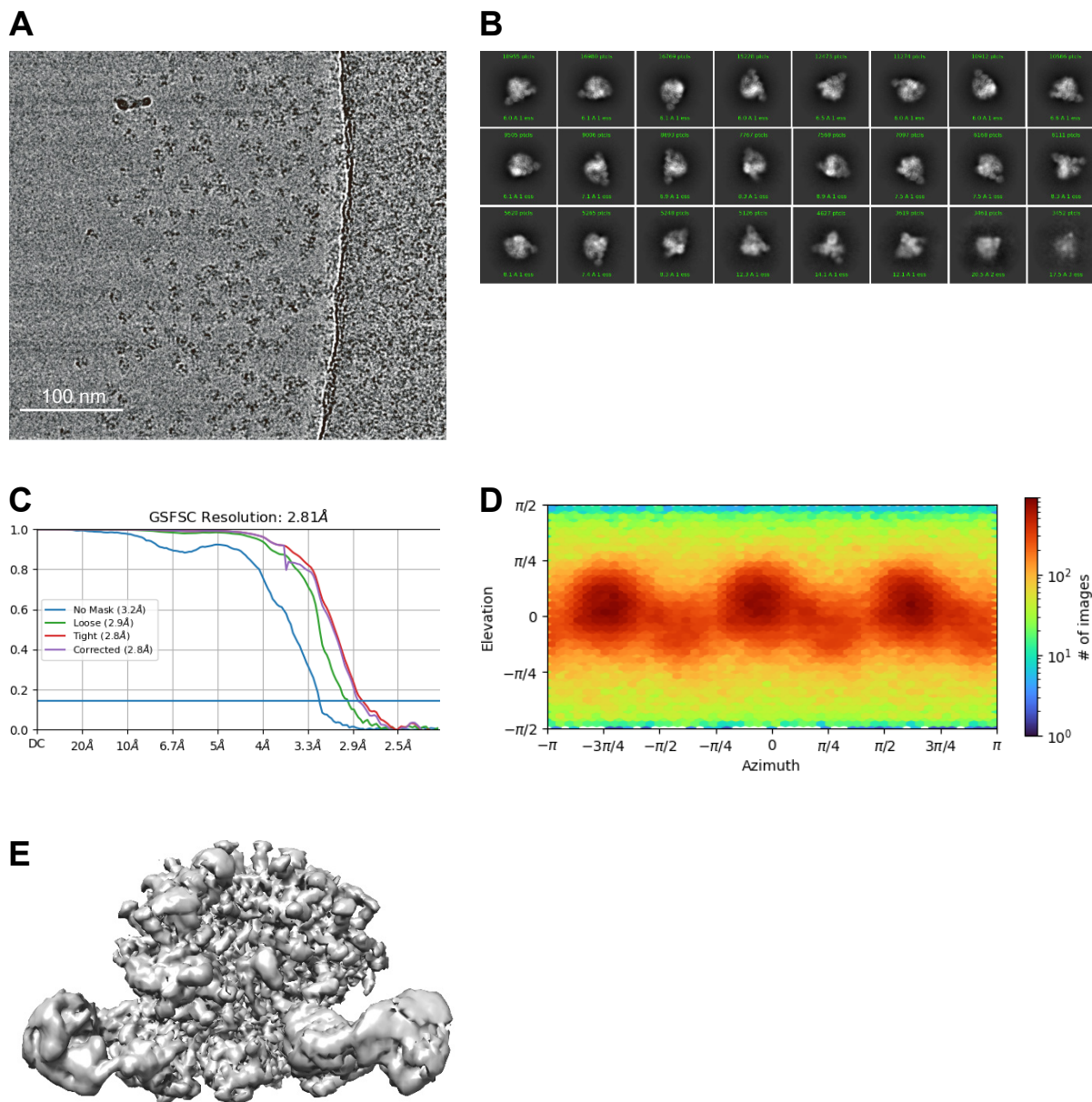


**Figure S4. Cryo-EM validation for 2C09 in complex with BG505 DS-SOSIP, related to Figure 3.**

(A) Representative micrograph. (B) 2D classes. (C) Fourier shell correlation (FSC) curves showing gold-standard FSC resolution at 2.81 Å. (D) Orientations of all particles used in the final refinement shown as a heatmap. (E) 3D reconstruction density map at 2.81 Å from non-uniform refinement with C3 symmetry, showing antibody Fab binding near the trimer base at the fusion peptide-site of vulnerability.



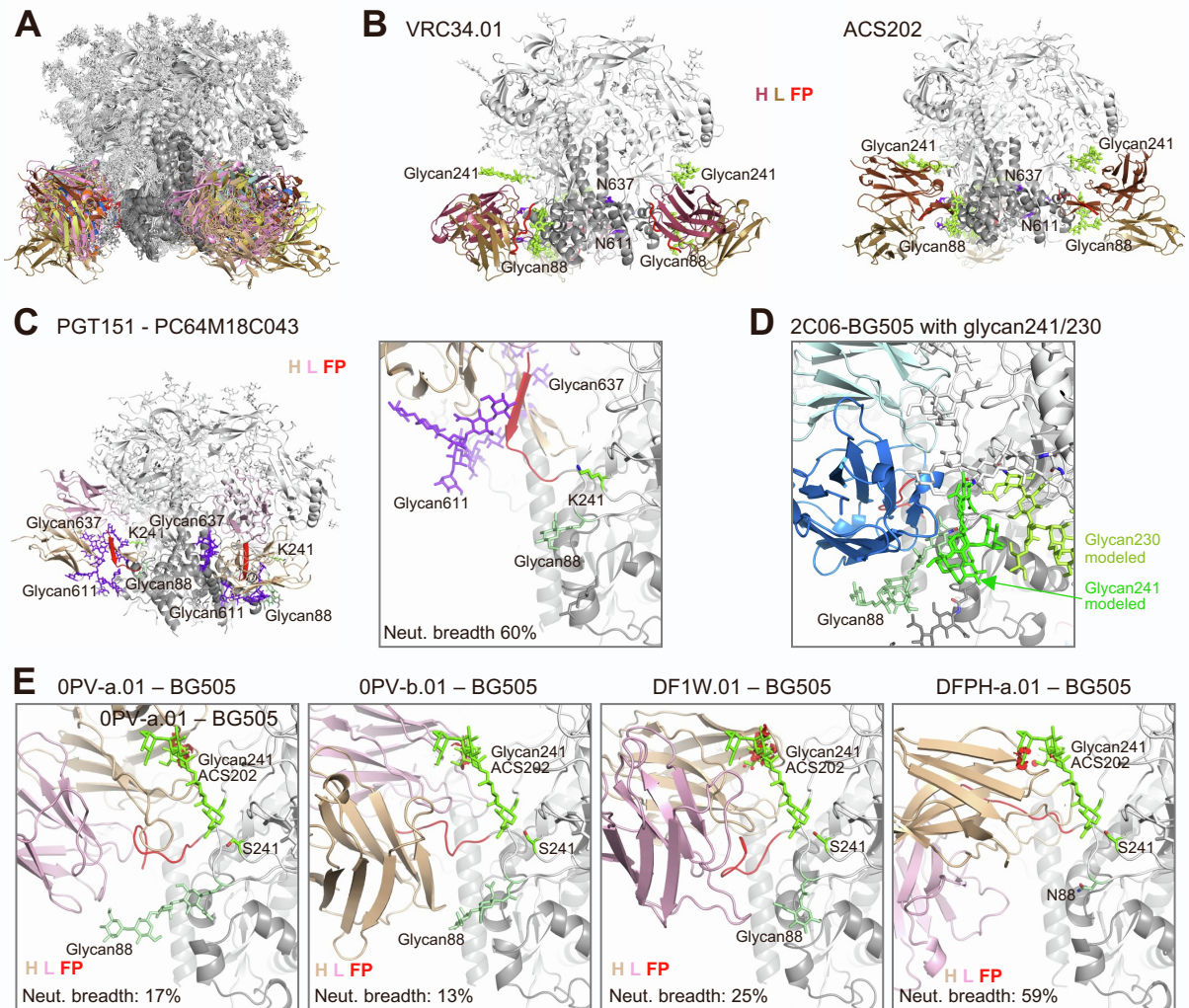


**Figure S5. Fusion peptide-directed antibodies (except for PGT151) bind at a similar location and interact favorably with glycan88 but variably with glycan241, related to Figure 5.**

(A) Structural superposition of fusion peptide-directed antibodies in complex with Env trimer. The structures, 2C06, 2C09, ACS202 (PDB: 6nc2), VRC34.01 (PDB: 6nc3), DFPH-a.01 (modeled based on DFPH-a.15 structure, PDB: 6n1w), DF1W-a.01 (PDB: 6mph), A12V163-a.01 (PDB: 6n1v), A12V163-b.01 (PDB: 6mpg), 0PV-a.01 (PDB: 6osy), 0PV-b.01 (PDB: 6ot1), 0PV-c.01 (PDB: 6nf2), and vFP16.02 (PDB: 6cdi), were aligned by one of the gp120 subunits (right).

(B) Binding of VRC34.01 and ACS202 involves both glycan88 and glycan241 (green sticks), but not glycan611 or glycan637, both not modeled in the structure, likely disordered. VRC34.01 and ACS202 bind in a similar location but with different orientations.

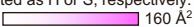
(C) PGT151 (PDB: 6dcq) binds to glycan611 and glycan637 (blue-purple sticks), away from glycan88 (green sticks) and the side chain of K241 (green sticks). Neutralization breadths were for IC<sub>50</sub> <50 μg/ml in the 208-strain panel.

(D) Structure of 2C06-BG505 complex with glycans at 241 and 230, as well as all other potential glycans modeled as mannose 5. With adjustment of glycan conformations, both glycans at 241 and 230 could be modeled without clashing with each other or with the antibody.

(E) Vaccine-elicited NHP or murine antibodies all bind at a similar location to that of VRC34.01 and ACS202. The aligned glycan241 from the ACS202 complex (green sticks) has some minor clashes with antibodies 0PV-a.01, 0PV-b.01, DF1W.01, and DFPH-a.01, shown as red disks in Pymol (<https://pymol.org/2/>). These clashes are from the terminal mannose residues and can be avoided by minor shifts of the glycan, unlike those observed in 2C06 and 2C09 and other vaccine-elicited antibodies shown in Figure 5.

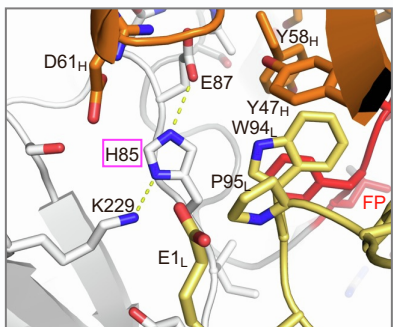
**A**

Position	Entropy	Most freq aa	2C06		2C09		A12V163-a.01		A12V163-b.01		VRC34.01 <sub>a</sub>		vFP16.02		0PV-c.01		
			Contact atoms	BSA	Contact atoms	BSA	Contact atoms	BSA	Contact atoms	BSA	Contact atoms	BSA	Contact atoms	BSA	Contact atoms	BSA	
512	0.082	Ala (96.5)	C, O	4.78	C, O	11.9	N, CA, C, O, CB	158.6	CA, C, O	20.1	N(H), CA, C, O, CB	127.3	N, CA, C, O(H), CB	161.6	N(H, S), CA, C, O, CB	83.1	
513	0.275	Val (80.6)	N, CA, C, O, CB, CG2	26.9	CA, C, O, CB, CG1, CG2	87.6	N, CA, C, O, CB, CG1, CG2	86.2	N, CA, C, O, CB	22.9	N(H), CA, C, O(H), CB, CG1, CG2	114.5	N(H), CA, C, O(H), CB, CG1, CG2	106.9	N(H), CA, C, O, CB, CG1, CG2	97.4	
514	0.226	Gly (84.9)	N, CA, C, O	19.9	N, CA	11.9	N(H), CA, C, O(H)	73.7	N, CA, C, O	46.4	N, CA, C, O	22.6	N(H), CA, C, O	42.6	N, CA, C, O(H)	90.7	
515	0.411	Ile (50.0)	N, CA, C, O, CB, CG1, CG2, CD1	75.6	N(H), C, O(H), CB, CG1, CG2, CD1	30.7	N, CA, C, O, CB, CG1, CG2, CD1	154.6	N, CA, C, O(H), CB, CG1, CG2, CD1	125.4	N(H), CA, C, O(H), CB, CG1, CG2, CD1	153.4	N, CA, C, O, CB, CG1, CG2, CD1	140.6	N, CA, C, O, CB, CG1, CG2, CD1	134.5	
516	0.023	Gly (99.0)	N, CA, C, O(H)	81.5	N(H), CA, C, O(H)	55.9	N, CA, C, O	25.1	N, CA, C, O	41.3	N, CA, C, O(H), CB, CG1, CG2	38.7	N, CA, C, O	38.2	N(H), CA, C, O(H)	67.1	
517	0.043	Ala (98.1)	N, CA, C, O, CB	31.1	N, CA, C, O, CB	36.3	N, CA, C, O, CB	44.8	N(H), CA, C, O, CB	108.9	N(H), CA, C, O(H), CB	46.9	N, CA, C, O, CB	40.3	N(H), CA, C, O(H), CB	70.3	
518	0.429	Val (45.1)	N, CA, C, O(H), CB, CG1, CG2	146.2	N, CA, O, CB, CG1, CG2	151.4	CA, C, CB, CG1, CG2	74.6	N, CA, C, O, CB, CG1, CG2	122.9	N, CA, C, O, CB, CG1, CG2	91	N, CA, CB, CG1, CG2	34	N(H), CA, C, O, CB, CG1, CG2	145.4	
519	0.183	Phe (85.9)	N, CA, C, O, CB, CG, CD1, CD2, CE1, CE2, CZ	106.4	N, CA, O, CB, CG, CD1, CD2, CE1, CE2, CZ	108.6	N, O, CG, CD1, CE1, CE2, CZ	67.9	N, CA, C, O, CB, CG, CD1, CD2, CE1, CE2, CZ	132.3	N(H), C, O(H), CB, CG, CD1, CD2, CE2	72.1	CB, CG, CD1, CD2, CE1, CE2, CZ	46.2	N(H), CA, C, O(H), CB, CD1, CD2, CE1, CE2, CZ	83.2	
520	0.144	Leu (90.8)	N, CA, O, CB, CG, CD1, CD2	45.5	N, O, CB, CD1	65	CA, C, CB, CG, CD1, CD2	63.6	N	6.02	N, CA, O(H)	47.7	CD1	17.2	N, CA, O, CB, CG, CD1, CD2	62.4	
535	0.472	Ile (47.6)	Met (17.6)	CG	5.52	SD, CE	17.7					CG	1.67	SD, CE	26.7		
85	0.733	Val (49.8)	His (2.5)	N, CA, O, CB, CG, CD2, ND1, CE1, NE2	67.9	N, CA, CB, CG, CD2, ND1, CE1, NE2	62.1	N, CA, C, O, CB, CG, CD2, ND1, CE1, NE2	94.6	N, CA, C, O, CB, CG, CD2, ND1, CE1, NE2	74.4	N, CB, CG1, CG2	40.9	N, CB, CG, CD2, ND1, CE1, NE2	43.2	N(H), O, CB, CG, CD2, ND1, CE1, NE2	69
87	0.573	Glu (52.7)	Glu (6.8)	CA, CB, CG, CD, OE1, OE2	77.3	CB, CG, CD, OE1, OE2(H, S)	85.6	N, CA, C, O, CB, CG, CD	46.2	N, CA, C, O, CB, CG, CD, OE1, OE2	77.3	CB, CG, CD, OE1, OE2	39.2	CG, OE1, OE2	46.7		
640	0.743	Gly (24.8)	Gln (1.7)	CA, C, O	19.2												
644	0.729	Thr (26.5)	Gly (1.7)														
648	0.547	Glu (54.9)	Glu (1.7)	N, CA, CB, CG, CD, OE1	23.2												
651	0.417	Asn (69.2)	Asn (1.7)	CB, CG, ND2	28.8												

a – Numbers in parentheses are the percentage frequency of the amino acid in the 2020 HIV-1 group M sequences.  
 b – Hydrogen bonds or salt bridges involved with the atom are designated as H or S, respectively.  
 c – BSA, buried surface area in Å<sup>2</sup> per residue calculated with PISA. 0  160 Å<sup>2</sup>  
 d – VRC34.01 in complex with AMC011 Env, which has a Val at position 85 instead of His.

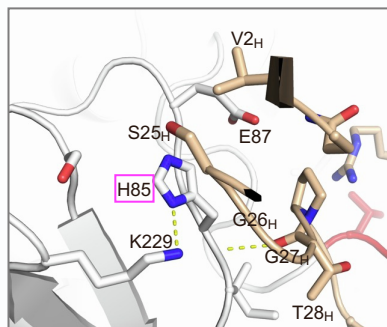
**B**

His85 interactions with 2C09



**C**

His85 interactions with 0PV-c.01



**D**

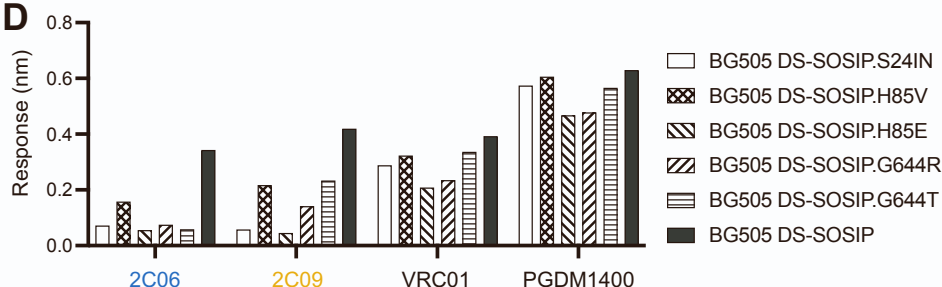


**Figure S6. Analysis of entropy and binding interactions of the epitope residues for 2C06 and 2C09 in comparison with other fusion peptide-directed antibodies, related to Figure 6.**

(A) Shannon entropy and contact surface areas of epitope residues for strain-specific and broadly neutralizing fusion peptide-directed antibodies. Residues analyzed include fusion peptide residues 512 to 520 and other residues involved in binding of 2C06 and 2C09 with normalized entropy above 0.4. Entropy values were calculated with Shannon Entropy-One ([https://www.hiv.lanl.gov/content/sequence/ENTROPY/entropy\\_one.html](https://www.hiv.lanl.gov/content/sequence/ENTROPY/entropy_one.html)) on the curated alignment of year 2020 HIV-1 M group Env of 5255 sequences (<https://www.hiv.lanl.gov/content/sequence/NEWALIGN/align.html>), and were normalized to have values between 0 and 1. Contact atoms and BSA were calculated with PISA ([https://www.ebi.ac.uk/msd-srv/prot\\_int/cgi-bin/piserver](https://www.ebi.ac.uk/msd-srv/prot_int/cgi-bin/piserver)).

(B) His85 has tight interactions with 2C09 heavy and light chain residues, similar to that in the 2C06 complex. (C) In 0PV-c.01, most interactions with H85 side chain are from heavy chain residues S25, G26, and G27. There is space and flexibility to accommodate other amino acids at position 85, despite large BSA with H85. (D) BLI assays for antibody binding to mutants of BG505 DS-SOSIP, S241N, H85V, H85E, G644R, and G644T.



**Table S1. Cryo-EM data and refinement statistics, related to Figures 2 and 3.**

	2C06	2C09
<b>EMDB ID</b>	EMD-29725	EMD-29731
<b>PDB ID</b>	8G4M	8G4T
<u>Data Collection</u>		
Microscope	FEI Titan Krios	FEI Titan Krios
Voltage (kV)	300	300
Electron dose (e <sup>-</sup> /Å <sup>2</sup> )	58.06	58
Detector	Gatan K3 BioQuantum	Gatan K2 Summit
Pixel Size (Å)	0.83	1.11
Defocus Range (µm)	-0.8/-2.0	-1.0/-2.5
Magnification	105,000	29,000
 <u>Reconstruction</u>		
Software	cryoSPARC v3.3.1	cryoSPARC v3.3.1
Particles	645,442	445,733
Symmetry	C1	C3
Resolution (Å) (FSC <sub>0.143</sub> )	2.95	2.81
 <u>Refinement</u>		
Software	Phenix 1.20	Phenix 1.20
Protein residues	2432	2437
Ligands	BMA: 7; NAG: 98; MAN: 14	BMA: 9; NAG: 105; MAN: 15
CC (box)	0.80	0.83
CC (mask)	0.88	0.88
R.m.s. deviations		
Bond lengths (Å)	0.003	0.004
Bond angles (°)	0.459	0.453
 <u>Validation</u>		
Molprobit score	1.55	1.51
Clash score	4.25	4.00
Rotamer outliers (%)	2.43	1.38
Ramachandran		
Favored regions (%)	97.78	96.62
Allowed regions (%)	2.22	3.38
Disallowed regions (%)	0	0

**Table S2. Epitope analysis for fusion peptide-directed antibodies in comparison to non-fusion peptide antibodies, related to Figure 6.**

Epitope entropy was calculated as BSA weighted average of normalized Shannon's entropy based on 208-virus panel for the epitope residues of each antibody. Percentage of epitope overlap was calculated as number of overlapping epitope residues divided by the number of epitope residues for the antibody with the least number of epitope residues of the two. Epitope residue was defined as residue with BSA>0. Fusion peptide-directed antibodies have substantial epitope overlap, and they have similar epitope entropies, except PGT151, which binds at a slightly different location and has a lower epitope entropy. Non-fusion peptide antibodies have variable epitope entropies that correlates with neutralization breadth.

Category	PDB ID	Antibody	Epitope entropy	Neut breadth	Epitope BSA (Å <sup>2</sup> )	Epitope overlap (%) with	
						2C06	2C09
Fusion peptide		2C06	0.29	<1%	1268	100	90
		2C09	0.26	<1%	1044	90	100
		6mpg A12V163-b.01	0.28	0%	1083	84	87
		6n1v A12V163-a.01	0.28	3%	1055	84	92
		6osy 0PV-a.01	0.26	17%	1108	71	71
		6ot1 0PV-b.01	0.26	13%	1017	67	57
		6nf2 0PV-c.01	0.27	23%	1320	62	71
		6mph DF1W-a.01	0.26	25%	1068	75	65
		6nc2 ACS202	0.30	26%	902	62	74
		6cdi vFP16.02	0.24	31%	1107	69	81
		6nc3 VRC34.01	0.27	50%	774	71	75
		6n1w DFPH-a.1	0.27	59%	1179	88	69
	5fuu PGT151	0.15	60%	1465	54	55	
V1V2	3u2s	PG9	0.38	81%			
	5v8l	PGT145	0.31	75%			
	5vgj	VRC38.01	0.46	29%			
Glycan-V3	5aco	PGT128	0.38	69%			
	5cez	PGT121	0.34	65%			
	4jm2	PGT135	0.47	34%			
	6ozc	2G12	0.40	25%			
CD4-binding site	5fyj	VRC01	0.25	90%			
	4yjd	VRC13.01	0.16	83%			
	4ydk	VRC16.01	0.18	55%			
	5f9o	8ANC131	0.20	53%			
	4jan	CH103	0.23	53%			
	5t3z	IOMA	0.23	50%			
	5vn8	b12	0.29	43%			
	4ye4	HJ16	0.51	31%			
Silent face	6bf4	VRC-PG05	0.60	28%			
Subunit	5cez	35O22	0.29	45%			
interface	5cix	8ANC195	0.21	67%			

**Table S3. Analysis of antibody-trimer interfaces, by CDRs, related to Figures 2 and 3.** Subunit interface buried surface areas ( $\text{\AA}^2$ ) were analyzed using PISA. Blank entries are 0, i.e. no binding interactions.

	Chain	Protomer 1		Protomer 2		Protomer 3		Subtotal
		A gp41	C gp120	B gp41	G gp120	F gp41	I gp120	
<b>2C06</b>	CDR H1	54.67						54.67
Antibody 1	CDR H2	164.67	129.49					294.16
(chains DE)	CDR H3	316.52	14.32			126.34		457.18
	L N-term		27.07					27.07
	CDR L1		87.45					87.45
	CDR L3	58.34	176.47					234.81
	FR L3		8.97					8.97
	DE total	594.2	443.77			126.34		1164.31
Antibody 2	CDR H1			72.27				72.27
(chains JK)	CDR H2			184.65	118.97			303.62
	CDR H3	204.07		280.25	13.11			497.43
	L N-term				7.71			7.71
	CDR L1				95.57			95.57
	CDR L3			59.48	176.94			236.42
	FR L3				7.66			7.66
	JK total	204.07		596.65	419.96			1220.68
Antibody 3	CDR H1					65.28		65.28
(chains HL)	CDR H2					198.22	122.92	321.14
	CDR H3			202		255.54	15.73	473.27
	L N-term						11.5	11.5
	CDR L1						92.69	92.69
	CDR L3					58.82	178.01	236.83
	FR L3						6.7	6.7
	HL total			202		577.86	427.55	1207.41
<b>2C09</b>	CDR H1	93.24						93.24
Antibody 1	CDR H2	164.88	98.03					262.91
(chains DE)	CDR H3	256.08	14.32					270.4
	L N-term		27.07					27.07
	CDR L1		83.25					83.25
	CDR L3	92.08	170.84					262.92
	FR L3		8.97					8.97
	DE total	606.28	402.48					1008.76
antibody	CDR H1			92.27				92.27
(chains JK)	CDR H2			164.61	100.5			265.11
	CDR H3			258.57	13.11			271.68
	L N-term				7.71			7.71
	CDR L1				83.33			83.33
	CDR L3			88.73	170.05			258.78
	FR L3				7.66			7.66
	JK total			604.18	382.36			986.54
Antibody	CDR H1					91.49		91.49
(chains HL)	CDR H2					166.05	98.03	264.08
	CDR H3					259.94	15.73	275.67
	L N-term						11.5	11.5
	CDR L1						83.74	83.74
	CDR L3					86.97	170.6	257.57
	FR L3						6.7	6.7
	HL total					604.45	386.3	990.75

**Table S4. Analysis of antibody-trimer interfaces, by trimer sequence segments, related to Figures 2 and 3.** Subunit interface buried surface areas ( $\text{\AA}^2$ ) were analyzed using PISA. Blank entries are 0, i.e. no binding interactions.

			Antibody 1 DE		Antibody 2 JK		Antibody 3 HL	
Epitope subregions			Heavy	Light	Heavy	Light	Heavy	Light
<b>2C06</b>								
Protomer 1	A gp41	FP 512-520	469.77	64.41	149.14			
		524-542	109.63					
		592-648						
	C gp120	79-88	125.14	276.3				
		glycan88	249.6					
		227+229		45.91				
Protomer 2	B gp41	FP 512-520	99.28		489.37	67.96	142.4	
		524-542			154.52			
		588-648						
	G gp120	79-88			119.21	292.67		
		glycan88			247.2			
		227+229				19.07		
Protomer 3	F gp41	FP 512-520	99.28		1180.1	379.7	455.95	67.28
		524-542					146.62	
		644-651						
	I gp120	79-88					125.64	299.58
		glycan88					246	
		227+229						20.52
	241	22.27						
Subtotal			1073.05	386.62	1180.1	379.7	1138.9	387.38
<b>2C09</b>								
Protomer 1	A gp41	FP 512-520	463.99	91.9				
		524-542	70.96					
		592-648						
	C gp120	85-88	125.14	279.91				
		glycan88	285					
		229		10				
Protomer 2	B gp41	FP 512-520	99.28		470.71	90.22		
		524-542			71.48			
		588-648						
	G gp120	85-88			101.4	279.55		
		glycan88			285			
		229				7.5		
Protomer 3	F gp41	FP 512-520	99.28		944.58	377.27	469.98	89.36
		524-542					71.83	
		644-651						
	I gp120	85-88					102.66	276.51
		glycan88					285	
		229					0.17	8.55
	241	14.1						
Subtotal			964.72	381.81	944.58	377.27	943.74	374.42



**Table S5. Frequency of N-glycosylation sites in HIV-1 Env sequences, related to Figure 5.** HIV-1 Env protein sequence alignment was from HIV sequence database (<https://www.hiv.lanl.gov/content/sequence/NEWALIGN/align.html>) M group without recombinants, year 2020, a total of 5255 sequences. The aligned sequences were input to N-GlycoSite (<https://www.hiv.lanl.gov/content/sequence/GLYCOSITE/glycosite.html>), excluding NP[ST] and first position N in NN[ST][ST], with HXB2 as reference sequence.

Position in sequence alignment	HXB2 sequence	HXB2 residue number	Number of sequences with N-glycan sequon	Frequency of N-glycosite	Position in sequence alignment	HXB2 sequence	HXB2 residue number	Number of sequences with N-glycan sequon	Frequency of N-glycosite	Position in sequence alignment	HXB2 sequence	HXB2 residue number	Number of sequences with N-glycan sequon	Frequency of N-glycosite	Position in sequence alignment	HXB2 sequence	HXB2 residue number	Number of sequences with N-glycan sequon	Frequency of N-glycosite
10	h	9	19	0.36	268	N	156	5030	95.72	541	N	301	4969	94.56	739	n	425	1	0.02
13	w	11	1	0.02	272	N	160	4741	90.22	542	n	302	74	1.41	756	s	440	1	0.02
14	r	12	1	0.02	273	l	161	3	0.06	544	r	304	1	0.02	758	q	442	1524	29.00
41	i	27	19	0.36	274	s	162	1	0.02	568	g	321	2	0.04	759	i	443	1	0.02
43	s	29	185	3.52	276	s	164	10	0.19	569	k	322	1	0.02	760	r	444	462	8.79
44	a	30	1	0.02	277	i	165	1	0.02	588	h	330	8	0.15	762	s	446	370	7.04
45	t	31	7	0.13	281	-	166	1	0.02	591	N	332	4207	80.06	764	N	448	4519	85.99
46	-	31	1	0.02	288	g	167	1	0.02	593	s	334	670	12.75	776	g	459	3	0.06
47	-	31	1	0.02	289	k	168	1	0.02	594	r	335	11	0.21	777	n	460	694	13.21
48	-	31	1	0.02	291	q	170	1	0.02	597	k	337	303	5.77	778	s	461	1101	20.95
52	-	31	3	0.06	292	k	171	10	0.19	598	w	338	1	0.02	779	n	462	1552	29.53
54	-	31	2	0.04	293	e	172	1	0.02	600	N	339	3615	68.79	780	N	463	1044	19.87
55	-	31	1	0.02	295	y	173	1	0.02	601	n	340	10	0.19	781	-	463	189	3.60
56	-	31	1	0.02	299	f	176	1	0.02	602	t	341	4	0.08	782	-	463	102	1.94
58	e	32	16	0.30	300	y	177	1	0.02	604	k	343	47	0.89	783	-	463	47	0.89
74	e	47	18	0.34	303	l	179	1	0.02	605	q	344	138	2.63	784	-	463	2	0.04
76	t	49	619	11.78	307	p	183	1	0.02	606	i	345	1	0.02	788	-	463	7	0.13
82	c	54	1	0.02	308	l	184	1	0.02	607	a	346	7	0.13	804	-	463	1	0.02
87	k	59	1	0.02	309	d	185	293	5.58	609	k	348	1	0.02	805	-	463	1	0.02
96	n	67	1	0.02	310	N	186	723	13.76	611	r	350	6	0.11	806	-	463	5	0.10
126	v	85	15	0.29	311	-	186	199	3.79	612	-	350	2	0.04	808	-	463	11	0.21
128	v	87	1	0.02	312	-	186	287	5.46	617	e	351	6	0.11	809	-	463	8	0.15
131	-	87	1	0.02	313	-	186	184	3.50	618	q	352	1	0.02	810	-	463	13	0.25
132	N	88	5186	98.69	314	-	186	95	1.81	620	g	354	378	7.19	811	-	463	16	0.30
136	n	92	23	0.44	315	-	186	34	0.65	621	-	354	14	0.27	812	-	463	13	0.25
155	k	97	20	0.38	316	-	186	12	0.23	622	-	354	5	0.10	813	-	463	23	0.44
156	n	98	2	0.04	317	-	186	8	0.15	623	-	354	6	0.11	814	-	463	43	0.82
173	d	113	5	0.10	318	-	186	12	0.23	624	-	354	1	0.02	815	-	463	51	0.97
180	c	119	1	0.02	319	-	186	10	0.19	628	-	354	3	0.06	816	-	463	50	0.95
184	-	122	1	0.02	320	-	186	9	0.17	630	-	354	4	0.08	817	-	463	127	2.42
188	-	125	1	0.02	322	-	186	3	0.06	631	-	354	7	0.13	818	-	463	1617	30.77
191	s	128	7	0.13	323	-	186	6	0.11	632	-	354	8	0.15	819	e	464	5	0.10
192	l	129	1	0.02	324	-	186	1	0.02	633	n	355	211	4.02	820	s	465	1101	20.95
193	k	130	3353	63.81	325	-	186	3	0.06	634	N	356	3992	75.97	833	n	478	4	0.08
195	t	132	55	1.05	326	-	186	1	0.02	635	k	357	25	0.48	843	v	488	1	0.02
196	d	133	872	16.59	328	-	186	1	0.02	636	t	358	232	4.41	855	t	499	1	0.02
197	l	134	167	3.18	329	-	186	1	0.02	637	i	359	3	0.06	952	q	567	1	0.02
198	k	135	1243	23.65	330	-	186	3	0.06	638	l	360	166	3.16	984	g	597	7	0.13
199	N	136	881	16.76	331	-	186	1	0.02	639	f	361	1	0.02	994	a	607	7	0.13
200	d	137	1268	24.13	332	-	186	2	0.04	640	k	362	2177	41.43	998	N	611	5179	98.55
201	t	138	824	15.68	334	-	186	3	0.06	642	-	362	3	0.06	999	a	612	1	0.02
202	n	139	760	14.46	335	-	186	3	0.06	643	q	363	304	5.78	1000	s	613	36	0.69
203	t	140	812	15.45	336	-	186	4	0.08	653	t	373	2	0.04	1003	-	615	11	0.21
204	N	141	778	14.80	337	-	186	8	0.15	655	h	374	1	0.02	1004	-	615	15	0.29
205	s	142	743	14.14	338	-	186	9	0.17	656	s	375	1	0.02	1005	-	615	3	0.06
206	-	142	466	8.87	339	-	186	16	0.30	662	e	381	1	0.02	1006	-	615	1	0.02
207	-	142	312	5.94	340	-	186	26	0.49	668	N	386	4523	86.07	1007	-	615	3	0.06
208	-	142	250	4.76	341	-	186	44	0.84	670	t	388	1	0.02	1009	-	615	1	0.02
209	-	142	160	3.04	342	-	186	104	1.98	672	q	389	2	0.04	1012	-	615	1	0.02
210	-	142	135	2.57	343	-	186	218	4.15	674	l	390	1	0.02	1013	-	615	2	0.04
211	-	142	111	2.11	344	-	186	301	5.73	675	f	391	1	0.02	1014	-	615	1	0.02
212	-	142	71	1.35	345	-	186	453	8.62	676	N	392	4100	78.02	1015	-	615	19	0.36
213	-	142	63	1.20	346	-	186	511	9.72	677	s	393	89	1.69	1016	N	616	4780	90.96
215	-	142	12	0.23	347	d	187	1505	28.64	678	t	394	216	4.11	1017	k	617	3	0.06
217	-	142	6	0.11	348	t	188	1490	28.35	679	w	395	94	1.79	1018	s	618	287	5.46
218	-	142	6	0.11	349	t	189	8	0.15	680	f	396	1387	26.39	1024	-	623	1	0.02
219	-	142	13	0.25	350	s	190	16	0.30	681	N	397	642	12.22	1025	-	623	1	0.02
220	-	142	6	0.11	353	l	193	1	0.02	682	s	398	1722	32.77	1026	N	624	36	0.69
221	-	142	15	0.29	355	s	195	7	0.13	683	t	399	381	7.25	1027	h	625	5077	96.61
222	-	142	2	0.04	356	c	196	4	0.08	684	w	400	382	7.27	1038	i	635	1	0.02
223	-	142	3	0.06	357	N	197	5145	97.91	685	s	401	518	9.86	1040	N	637	5082	96.71
224	-	142	2	0.04	358	t	198	1	0.02	686	t	402	1112	21.16	1043	s	640	1	0.02
225	-	142	4	0.08	374	k	207	2	0.04	687	e	403	582	11.08	1048	s	644	1	0.02
226	-	142	3	0.06	395	k	227	1	0.02	688	g	404	598	11.38	1052	e	648	1	0.02
227	-	142	4	0.08	397	n	229	59	1.12	689	s	405	451	8.58	1083	n	656	1	0.02
228	-	142	4	0.08	401	-	229	1	0.02	690	N	406	301	5.73	1094	k	665	5	0.10
231	-	142	2	0.04	402	N	230	2153	40.97	691	n	407	262	4.99	1101	n	671	1	0.02
232	-	142	1	0.02	404	t	232	86	1.64	692	t	408	237	4.51	1104	N	674	687	13.07
233	-	142	1	0.02	407	N	234	4098	77.98	693	-	408	102	1.94	1130	v	698	1	0.02
236	-	142	1	0.02	411	t	236	10	0.19	694	-	408	41	0.78	1142	n	706	5	0.10
238	-	142	2	0.04	413	p	238	7	0.13	696	-	408	4	0.08	1157	-	718	5	0.10
239	-	142	5	0.10	416	N	241	5072	96.52	700	-	408	1	0.02	1188	r	740	1	0.02
240	-	142	9	0.17	440	s	256	1	0.02	703	-	408	1	0.02	1189	d	741	6	0.11
241	-	142	21	0.40	441	t	257	1	0.02	706	-	408	1	0.02	1190	r	742	4	0.08
242	-	142	38	0.72	447	N	262	5220	99.33	709	-	408	3	0.06	1191	d	743	245	4.66
243	-	142	31	0.59	449	s	264	4	0.08	710	-	408	2	0.04	1192	r	744	3	0.06
244	-	142	54	1.03	452	e	267	1	0.02	712	-	408	2	0.04	1195	i	746	6	0.11
245	-	142	52	0.99	453	e	268	41											